Substantial maturity influence on carbon and hydrogen isotopic composition of *n*-alkanes in sedimentary rocks

Galina Vinnichenko [a*], Amber J.M. Jarrett [b], Lennart M. van Maldegem [a], Jochen J. Brocks [a*]

[a] *Research School of Earth Sciences, The Australian National University, Canberra, Australian Capital Territory 2601, Australia*

[b] *Geoscience Australia, Canberra, Australian Capital Territory 2601, Australia*

*Corresponding authors: galina.vinnichenko@anu.edu.au and jochen.brocks@anu.edu.au

ABSTRACT

Carbon ($\delta^{13}C$) and hydrogen ($\delta^{2}H$) compound-specific isotope analyses on sedimentary hydrocarbons are widely used for ecological reconstructions and oil-source rock or oil-oil correlations. However, the effects of thermal alteration on isotopic composition are not fully understood, potentially imparting a bias on interpretation of older and more mature sedimentary sequences. We measured $\delta^{13}C$ and $\delta^{2}H$ of *n*-alkanes in 23 extracted bitumens from the 1.64 Ga Paleoproterozoic Barney Creek Formation in the southern McArthur Basin, Australia. The samples cover a wide range of thermal maturities with calculated vitrinite reflectance (Rc) values from 0.4% to 1.3%. Our results illustrate that while $\delta^{13}C$ of kerogen remains relatively constant, the $\delta^{13}C$ and $\delta^{2}H$ of *n*-alkanes have a strong positive correlation with thermal maturity. Average $\delta^{13}C_{alk}$ increase by 6.8‰ and $\delta^{2}H_{alk}$ by 69‰ among the samples in the analysed maturity range. At the same time, the carbon isotopic offset between *n*-alkanes and kerogen ($\Delta\delta^{13}C_{alk–ker}$) climbs from 1.3‰ to 8.5‰ with increasing maturity. Therefore, the substantial maturity influence on stable carbon and hydrogen isotopes of *n*-alkanes must be considered in palaeoecological and petroleum correlation studies. In the initial stages of maturation, *n*-alkanes from the Barney Creek Formation display increasingly positive "isotope slopes" in plots of $\delta^{13}C_{alk}$ against carbon number. However, with further maturation, the slopes became increasingly negative. The isotope slope inversion indicates that the dominant mechanisms for *n*-alkane generation and

degradation changed during the progression from early diagenesis to metagenesis. Numerical models suggest that the formation of positive and negative isotope slopes may be driven by the balance of the formation of *n*-alkanes from kerogen and their subsequent degradation, and by dependence of the degradation rate constant *k* on *n*-alkane chain length.

Keywords: Precambrian, McArthur Basin, Compound-specific isotope analysis (CSIA), $\delta^{13}C_{ker}$, biomarkers, Rock-Eval pyrolysis

1. Introduction

Compound-specific isotope analysis (CSIA) provides valuable information about biological sources of individual compounds, carbon cycling and geological processes in ancient sedimentary environments (Murray et al., 1994; Rooney et al., 1998; Odden et al., 2002; Sessions, 2016). CSIA is also a successful tool for oil-source rock and oil-oil correlations in Phanerozoic sequences (Pedentchouk and Turich, 2018). However, limited CSIA measurements are available for Precambrian samples, mainly due to the rare preservation of lipid biomarkers in rocks of this age (e.g., French et al., 2015).

One of the widely used approaches for CSIA on ancient sediments is tracking the differences between isotopic composition of *n*-alkyl lipid remains (*n*-alkanes), breakdown products of chlorophyll (pristane and phytane), and total organic carbon (e.g., Logan et al., 1995; Close et al.,

2011; Williford et al., 2011; Schinteie and Brocks, 2017; van Maldegem, 2017). Typical Phanerozoic carbon isotope signatures on average follow the biosynthetic fractionation pattern with *n*-alkanes being ~4.5‰ ^{13}C-depleted relative to kerogen (Hayes, 2001) (throughout the text, the terminology isotopically 'depleted or enriched' refers to ^{13}C-depleted or ^{13}C-enriched). Inverse to this isotopic ordering, Proterozoic organic matter is characterised by a ~1.5‰ ^{13}C-enrichment of extractable *n*-alkanes relative to kerogen and consequently by positive values of $\Delta\delta^{13}C_{alk-ker}$ (Logan et al., 1995, 1997).

Logan et al. (1995) suggested that this inverse δ^{13}C pattern globally occurred in the Proterozoic through intensive heterotrophic reworking of slowly sinking primary biomass by bacteria and preferential preservation of heterotrophic lipids; whereas in the Phanerozoic, faster-sinking fecal pellets produced by multicellular organisms preserve the signatures of primary biomass. An alternative explanation was proposed by Close et al. (2011). In their mixed community model for the Proterozoic, relatively ^{13}C-enriched prokaryotic phytoplankton represent major input for preserved lipids (e.g., *n*-alkanes), whereas kerogen dominantly retains the isotopically depleted signatures of eukaryotic biomass. A recent study by van Maldegem (2017) showed that changes in redox and community can affect δ^{13}C systematics, supporting elements of both existing models. However, based on highly variable $\Delta\delta^{13}C_{alk-ker}$ values across different Precambrian sedimentary basins, the author suggested that the inverse δ^{13}C pattern between *n*-alkanes and kerogen is not a universal Proterozoic signal.

The hydrogen isotopic (δ^2H) composition of *n*-alkanes is controlled by a combination of environmental, biological, physical and chemical processes (Sessions, 2016). For thermally immature samples, a wide range of the δ^2H values can reveal information about water chemistry (e.g., meteoric, marine), organic matter source (e.g., marine algae vs terrestrial plants, or autotrophs vs heterotrophs) and biosynthetic fractionations (Sessions, 2016 and References therein). However, hydrogen exchange with water or clay minerals during diagenesis might complicate the original δ^2H signatures and lead to ^2H-enrichment of organic matter (Alexander et al., 1982; Sessions et al., 2004).

Over geological time, the primary carbon and hydrogen isotopic composition of bitumens can be significantly altered by diagenetic and catagenetic processes and especially by increasing thermal maturity (e.g., Clayton, 1991; Clayton and Bjorøy, 1994; Schimmelmann et al., 1999; Dawson et al., 2005, 2007; Radke et al., 2005; Tang et al., 2005; Pedentchouk et al., 2006; Maslen et al., 2012; Cheng et al., 2015; Sessions, 2016). For example, Tang et al. (2005) used anhydrous, closed-system pyrolysis experiments to show that thermal alteration alone can increase δ^2H_{alk} by ~50‰ and $\delta^{13}C_{alk}$ by ~4‰ at vitrinite reflectance equivalent values of 1.5%. Several Phanerozoic studies supported these experiments by showing a trend of increasing δ^2H of *n*-alkanes by up to ~71‰ with increasing maturity (e.g., Li et al., 2001; Dawson et al., 2005, 2007; Radke et al., 2005; Pedentchouk et al., 2006; Maslen et al., 2012), as well as $\delta^{13}C_{alk}$

values enriched by 2.0–4.5‰ in more mature samples (e.g., Clayton and Bjorøy, 1994; Odden et al., 2002; Dawson et al., 2007; Cheng et al., 2015). However, the number of studies that determine the maturity effect on $\delta^{13}C_{alk}$ and $\delta^{2}H_{alk}$ in natural systems is limited. Additionally, to our knowledge, there are no studies for the Phanerozoic and Precambrian that investigate $\delta^{13}C_{alk}$ across a wide range of maturities while keeping organic matter source constant. In this field-based study, we present the results of CSIA on extracted bitumens from the 1.64 Ga Barney Creek Formation (Fm) in the southern McArthur Basin, Australia. Since the Barney Creek Fm has a relatively constant organic matter source and covers a wide maturity range across the basin, we aim to test the effects of thermal alteration on Proterozoic carbon and hydrogen isotopic compositions of *n*-alkanes.

2. Geological setting and samples

The McArthur Basin is located in northern Australia and contains a Paleoproterozoic–Neoproterozoic succession of carbonate and siliciclastic rocks with minor volcanic horizons (Ahmad et al., 2013; Munson, 2016). The focus of this study is on the southern part of the basin, where the Paleoproterozoic section is stratigraphically subdivided into the Tawallah and McArthur groups (Jackson et al., 1987). The McArthur Group (~1690 to ~1614 Ma) is represented by shallow to deep marine succession of carbonates, shales, and sandstones (Jackson et al., 1987; Kunzmann et al.,

2019). The 1640 ± 4 Ma Barney Creek Fm of the McArthur Group comprises laminated dolomitic, carbonaceous and pyritic siltstone and shale (Jackson et al., 1987; Page and Sweet, 1998). The Barney Creek Fm is of particular scientific interest because it hosts potential petroleum resources (Powell et al., 1987; Johnson et al., 2013), world class Zn-Pb-Ag deposits, including the McArthur River 'HYC' Mine (Eldridge et al., 1993; Ireland et al., 2004), and it also contains indigenous lipid biomarkers of Paleoproterozoic age (Brocks et al., 2005).

For the current study, a total of 23 Barney Creek Fm samples at different levels of maturity (assessed using hydrocarbon parameters and Rock-Eval pyrolysis) were selected for CSIA and organic carbon isotope analyses (Table 1). Samples were collected from four open-source drill cores (LV09, GR7, BB5, BB6; Fig. 1), stored at the Northern Territory Geological Survey core library in Darwin, Australia. The unmineralized HYC hanging wall (182 m, 157 m and 94 m above the ore body) and foot wall were also sampled from two drill holes, BS024-01 and MRM 2012-03. These unmineralized HYC samples were selected to avoid hydrothermal alteration effects. We further included published $\delta^{13}C$ and $\delta^{2}H$ values from five HYC ore body samples (Williford et al., 2011).

3. Methods

3.1. Biomarker analysis

153 Biomarker analysis was performed at the Australian National
154 University and followed protocols allowing recognition and removal of
155 contamination (e.g., Brocks et al., 2008; Brocks, 2011; French et al., 2015;
156 Vinnichenko et al., 2020). Laboratory contaminants remained below
157 detection limits in the cumulative system blanks that experienced the whole
158 sequence of procedures along with samples. Since contamination from
159 drilling fluids can affect the results of CSIA (Schinteie et al., 2019), the
160 syngeneity of biomarkers was assessed by comparison of exterior and
161 interior (E/I) hydrocarbon contents (Brocks et al., 2008). Therefore, ~3 mm
162 of all external surfaces were removed using a solvent-cleaned precision
163 diamond wafering saw (Buehler IsoMet 1000) or a wet table saw (Nortel
164 Machinery Inc.), depending on sample size and shape. Then the exterior (E)
165 and interior (I) rock portions were ground to < 240 mesh powder using a
166 clean Rocklabs iron puck mill. Later, E and I rock powders were extracted
167 with a Dionex Accelerated Solvent Extractor (ASE 200) using 90% DCM and
168 10% methanol. Prior to fractionation, elemental sulfur was removed from
169 HYC extracts by filtration over freshly precipitated elemental copper. All
170 extracted bitumens were fractionated into saturated, aromatic, and polar
171 fractions using microcolumn (Pasteur pipette) chromatography over
172 annealed and dry-packed silica gel (7 cm). Saturated hydrocarbons were
173 eluted with 1.5 ml of *n*-hexane, aromatic hydrocarbons with 4 ml of *n*-
174 hexane:DCM (1:1, v/v) and polar hydrocarbons with 3 ml of DCM:methanol
175 (1:1, v/v). Gas chromatography–mass spectrometry (GC–MS) analyses were

carried out on an Agilent 6890 GC coupled to a Micromass Autospec Premier double-sector MS. The GC was equipped with a 60 m DB-5MS capillary column (0.25 mm ID, 0.25 μm film thickness; Agilent) and used helium as the carrier gas at a constant flow rate of 1 ml min^{-1}. Full Scan analyses were performed for saturated and aromatic fractions. Based on E/I criteria (e.g., Brocks et al., 2008), all analysed interior fractions contained indigenous biomarkers.

3.2. Compound-specific isotope analyses ($\delta^{13}C$ and $\delta^{2}H$)

Prior to CSIA, *n*-alkanes were separated from the saturated fractions (Fig. 2) using 0.5 mg of 5 Å zeolite molecular sieve (Grace Davison), which was activated at 300 ºC for 9 h. The molecular sieve and corresponding saturated fractions were combined with 3.5 ml of cyclohexane, sealed, vigorously mixed and kept overnight at 90 ºC on a hot plate. The sieve was filtered, washed with cyclohexane, air-dried for 2–3 h and digested in HF (32%, 3 ml) to release the *n*-alkanes, which were further extracted with 3 ml *n*-hexane. Total ion chromatograms of separated *n*-alkane fractions illustrate that branched/cyclic compounds and unresolved complex mixture were successfully removed during molecular sieving (Fig. 2).

Stable carbon and hydrogen isotopic compositions of individual *n*-alkanes were measured at Geoscience Australia. For carbon isotopes, the instrument comprised a Thermo Trace gas chromatograph (GC) connected to a Finnigan MAT 253 isotope ratio mass spectrometer (IRMS) via a

combustion furnace and water-removal assembly. The on-column injector temperature was held at 150 ºC. The 1 µl of pentane solution with sample *n*-alkanes was injected either manually or with the GC PAL autosampler. Individual hydrocarbons were quantitatively converted to CO_2 and H_2O in the combustion reactor operated at 940 °C. Water was removed using a tubular Nafion™ membrane swept with helium. The GC was equipped with a DB-5 fused silica column (60 m × 0.32 mm ID, 0.25 µm film thickness). The oven was maintained at 40 °C for 4 min, ramped to 220 °C at 6 °C/min and then to 310 °C at 8 °C/min with a hold of 40 min. A mixture of perdeuterated *n*-C_{16} ($\delta^{13}C$ = –28.68‰), *n*-C_{20} ($\delta^{13}C$ = –34.04‰), and *n*-C_{24} ($\delta^{13}C$ = –26.85‰) alkanes was co-injected or separately injected with the sample. In general, a precision of less than 0.3‰ was obtained for perdeuterated *n*-alkanes with minimal background. Hydrogen isotopes were obtained using a Thermo Scientific Delta V Advantage IRMS, which was linked to Trace GC-TC. Before analysis, background scans and zero enrichment were performed to monitor the day-to-day performance of the GC-TC-IRMS system as a routine daily procedure. The H_3^+ factor (< 10) was also calculated to ensure the linearity of results with responses within 0.5 to 10 V. Hydrocarbon components were resolved using a DB-5 capillary column (60 m × 0.32 mm ID, 0.25 µm film thickness) with Ultra High Purity (UHP) helium as a carrier gas at a constant flow rate of 1.2 ml min^{-1}. The on-column injector temperature was held at 150 ºC. The oven was maintained at 40 °C for 8 min, ramped to 200 °C at 10 °C/min and then to 310 °C at 8

°C/min with a hold of 40 min. The 2 µl of pentane solution with sample *n*-alkanes (more concentrated than for carbon isotopes) was injected either manually or with the GC PAL autosampler. A mixture of C_{20} (δ^2H = –177.8‰), C_{22} (δ^2H = –218.8‰), and C_{25} (δ^2H = –194.8‰) fatty acid methyl ester was separately injected with the sample as a standard to check the accuracy and repeatability of the GC-TC-IRMS system. The $\delta^{13}C$ and δ^2H values are reported in per mil (‰) notation relative to VPDB and VSMOW respectively. All analyses were run as a minimum in duplicate with an average standard deviation of individual compounds of 0.13‰ for $\delta^{13}C$ and 2‰ for δ^2H.

3.3. Organic carbon isotope analyses

Organic carbon isotope analyses of kerogen ($\delta^{13}C_{ker}$) for LV09 samples followed the methods described in Stüeken (2013) and Kipp et al. (2018), and were measured at the IsoLab facilities in the Department of Earth and Space Sciences of the University of Washington. Rock powders were decarbonised with 6 N HCl, then samples were rinsed in 18 MΩ DI-H_2O and dried in an oven at 60 °C. Carbonate-free powders were analysed with a Costech ECS 4010 Elemental Analyser coupled to a Thermo Finnigan MAT 253 continuous flow IRMS.

Kerogen isolation for BB5, BB6 and HYC samples was performed at Geoscience Australia following the in-house protocol. The $\delta^{13}C_{ker}$ was

244 measured with a Thermo Scientific MAT 253 IRMS for BB5 and BB6
245 samples, and with Sercon 20-20 combustion IRMS for HYC samples.
246
247 *3.4. Rock-Eval pyrolysis*
248 Total organic carbon (TOC) content and Tmax were measured on bulk
249 rock powders using a Rock-Eval 6 Turbo™ (Vinci Technologies, France) at
250 Geoscience Australia for BB5 and BB6 samples and Lomonosov Moscow
251 State University for LV09 and HYC samples.
252
253 *3.5. Numerical simulation of* n-*alkane degradation*
254 To assess the trajectory of *n*-alkane concentrations and $\delta^{13}C$-profiles
255 with increasing maturation, we constructed simple numerical models. The
256 annotated code and accessory files are available in the Supplementary
257 Information. Input variables include initial concentrations of C_1 to C_{33} *n*-
258 alkanes (in moles of carbon) and their carbon isotopic composition $\delta^{13}C$ vs
259 VPDB. The models consider three principal mechanisms of *n*-alkane
260 degradation and formation that may run in parallel: (1) Cleavage of *n*-
261 alkanes along the carbon chain to shorter molecules that are returned to the
262 reactant pool. The rate constant k_h (*h* = homolytic) and the $^{13}C/^{12}C$
263 fractionation factor α_h were assumed to be identical for each C–C bond
264 within individual *n*-alkanes, except for terminal $–CH_2–CH_3$ bonds, which
265 were neglected due to much higher activation energies of cleavage (Tang et
266 al., 2000; Watanabe et al., 2001). In the input parameter file, rate constants

267 $k_h(n)$ were set for each *n*-alkane homologue with carbon number *n*. For
268 instance, to simulate thermal degradation of *n*-alkane homologues in a
269 radical chain reaction in the gas phase, rate constants were set to follow the
270 established equation $k_h \sim (n-2)\times(n-3)^{1/2}$ (Watanabe et al., 2001). (2) The
271 second type of reaction 'isomerizes' *n*-alkanes into new products and
272 channels them into an 'isomer pool' but does not generate shorter *n*-alkanes.
273 These reactions have the rate constant k_i (*i* = isomerization) and $^{13}C/^{12}C$
274 fractionation factor α_i. In the reaction examined in more detail in this
275 manuscript, k_i was independent of *n*-alkane chain length *n*. (3) The third
276 type of reaction is the generation of new *n*-alkanes through cleavage of *n*-
277 alkyl moieties from kerogen. This reaction was simulated by cleaving *n*-C_{33}
278 residues along the chain assuming that all C–C bonds have the same
279 activation energy, except the terminal $–CH_2–CH_3$ bonds, which were
280 neglected (see above).
281
282 **4. Results**
283 *4.1. Biomarker distribution, thermal maturity and Rock-Eval data*
284 Extracted Barney Creek Fm bitumens from drill core LV09 (*n* = 12)
285 illustrate typical mid-Proterozoic (1.8–0.8 Ga) hydrocarbon distributions
286 including a large unresolved complex mixture, relatively high
287 methylalkane/*n*-alkane ratios, lack of steranes and prevalence of hopanes
288 and aromatic carotenoids (Brocks et al., 2005). The unimodal distribution of
289 *n*-alkanes ranges from C_{10} to C_{32} with a maximum at C_{14} to C_{20} (Fig. 2). The

ratio of pristane and phytane (Pr/Ph) varies slightly between 0.3 and 0.6 and is consistent with minimal oxygen exposure of organic matter (Peters et al., 2005). Although samples from drill cores GR7, BB5, and BB6 and the HYC mine are too mature for preservation of polycyclic terpanes and carotenoids derivatives, the extracts demonstrate a non-biodegraded unimodal distribution of *n*-alkanes in the range C_{10}–C_{30} with a maximum at C_{14}–C_{16} and elevated methylalkane/*n*-alkane ratios compared with LV09 extracts (Fig. 2).

The maturity level of Barney Creek Fm bitumens was assessed using the methylphenanthrene distribution factor (MPDF) (Kvalheim et al., 1987) (Table 1). Calculated vitrinite reflectance equivalent values Rc(MPDF) indicate variable thermal maturities that range from immature to early mature in LV09 (Rc = 0.44–0.71%), through the main oil window in GR7, BB5, and BB6 (Rc = 0.64–1.1%), and within the beginning of the gas window in the unmineralized HYC samples (Rc = 1.1–1.3%). Saturated hydrocarbon parameters based on polycyclic terpanes could not be applied in the current study since the required compounds such as hopanes were not detected in the more mature samples.

The results of Rock-Eval pyrolysis are summarized in Table 1. Based on the classification scheme of Peters and Cassa (1994), the Barney Creek Fm has fair to excellent organic richness with TOC between 0.35% and 4.7% (Table 1). Since the hydrogen index (HI) is probably underestimated in the samples with low TOC due to mineral matrix effects (Espitalié et al., 1980;

313 Dahl et al., 2004), in the following we only consider HI values in the samples
314 with TOC > 1%. In the least mature LV09 drill core with Tmax values from
315 424 °C to 438 °C, HI falls in the range 344–515 mg HC/g TOC and indicates
316 predominantly oil- and gas-prone marine kerogen (Table 1). In more mature
317 BB5, BB6 and HYC samples, HI illustrates much lower values of 18–64 mg
318 HC/g TOC (Table 1). S2 peaks of LV09, BB5 and unmineralized HYC
319 samples are well-formed Gaussian peaks (Supplementary Fig. S1a–c). Tmax
320 values for these samples vary from 424 °C to 468 °C (Table 1) and correlate
321 positively with Rc(MPDF) ($R^2 = 0.72$, $p = 0.0015$). Accordingly, the
322 methylphenanthrene-based maturity parameter and bulk rock Tmax are
323 consistent and demonstrate immature to late mature source rock.
324 Production index (PI) values around 0.1 for low maturity LV09 samples and
325 ≤ 0.3 for more mature BB5 and HYC samples suggest largely
326 uncontaminated source rocks (Peters and Cassa, 1994). Oil saturation
327 indices (S1/TOC) less than 100 mg of oil per gram of TOC indicate that all
328 analysed samples are unaffected by migrated hydrocarbons (Jarvie, 2012).
329 Tmax was also measured for BB6 samples. However, the results were not
330 included in this study due to unreliable pyrograms displaying broad bimodal
331 S2 peaks (Supplementary Fig. S1d) and anomalously low Tmax. Such S2
332 shapes are common for heavy ends of bitumen, migrated oil, or drilling
333 additives (Peters, 1986). Most probably, bulk BB6 rock powders used for
334 Rock-Eval pyrolysis were affected by surficial contamination. Nevertheless,
335 based on rigorous assessment of biomarker syngeneity using

336 Exterior/Interior experiments (Brocks et al., 2008), the interior fractions of
337 BB6 samples used for CSIA measurements remain unaffected by
338 contamination.
339
340 *4.2. Stable carbon isotopes*
341 The stable carbon isotopic composition of Barney Creek Fm kerogen
342 ($\delta^{13}C_{ker}$) is relatively constant across the Southern McArthur Basin, ranging
343 from –32.5‰ to –33.5‰ in LV09, from –32.6‰ to –34.4‰ in BB5 and BB6,
344 and from –33.1‰ to –34.0‰ in the unmineralized HYC samples (Table 1).
345 These values are also consistent with previously published $\delta^{13}C_{ker}$
346 measurements of the Barney Creek Fm (Powell et al., 1987; Williford et al.,
347 2011).
348 The carbon isotopic composition of *n*-alkanes ($\delta^{13}C_{alk}$), however, varies
349 more widely. It ranges from –29.6‰ to –32.6‰ for LV09, from –26.9‰ to –
350 27.5‰ for BB5, from –27.8‰ to –30.2‰ for BB6 and from –24.1‰ to –30.3‰
351 for HYC samples (Fig. 3a, Table 2). Most LV09 samples display an increase
352 of $\delta^{13}C_{alk}$ values by up to 3.5‰ with increasing carbon number in the range
353 *n*-C_{12}–C_{31}, while no clear trend was observed for the BB5 and BB6 drill
354 cores. Conversely, $\delta^{13}C_{alk}$ values in HYC samples generally decrease with
355 increasing *n*-alkane carbon number (Fig. 3a).
356 The discussion will focus on the non-weighted average of $\delta^{13}C$ of *n*-
357 alkanes in the range *n*-C_{16} to *n*-C_{23} (Table 1), as carbon isotope data are
358 available within that range for all samples. The average $\delta^{13}C_{alk}$ of *n*-C_{16}–C_{23}

for the Barney Creek Fm dataset increases from –31.8‰ to –25.0‰ with increasing Rc(MPDF). Similarly, the carbon isotopic offset between *n*-alkanes and kerogen ($\Delta\delta^{13}C_{alk-ker}$) increases from 1.3‰ in the early mature LV09 samples to 8.5‰ in the late mature HYC samples. Rc(MPDF) shows significant positive linear correlations with both $\Delta\delta^{13}C_{alk-ker}$ ($R^2 = 0.80$, $p < 0.00001$) and $\delta^{13}C_{alk}$ ($R^2 = 0.80$, $p < 0.00001$) (Fig. 4a,c). Previously published carbon isotope values for HYC bitumens (Williford et al., 2011), included in Fig. 4, fall on the trend line.

4.3. Stable hydrogen isotopes

The stable hydrogen isotopic composition of Barney Creek Fm *n*-alkanes (δ^2H_{alk}) is represented in Table 3 and Fig. 3b. Analysed samples show progressive enrichment in $^2H_{alk}$ with increasing chain length of *n*-alkanes. To remain consistent with the reported average $\delta^{13}C_{alk}$ values, we use non-weighted average δ^2H_{alk} for *n*-C_{16} to *n*-C_{23}. Average δ^2H_{alk} of *n*-$C_{16–}C_{23}$ varies from –103‰ to –120‰ for LV09, from –115‰ to –117‰ for GR7, from –87‰ to –96‰ for BB6, reaches –88‰ for BB5 and from –75‰ to –51‰ for HYC samples (Table 1). Similar to carbon isotopes, average δ^2H_{alk} yields a strong linear correlation ($R^2 = 0.74$, $p < 0.0001$) with Rc(MPDF) across the sample set (Fig. 4d). Additionally, δ^2H_{alk} correlates positively with $\delta^{13}C_{alk}$ ($R^2 = 0.83$, $p < 0.00001$, not shown).

5. Discussion

382 *5.1. Thermal maturity*

383 Based on Rc(MPDF), the Barney Creek Fm displays a wide range of
384 thermal alteration intensities, from immature to the beginning of the gas
385 window (Rc = 0.44–1.3%), with increasing maturity in the following order:
386 LV09, GR7, BB6 and BB5, unmineralized HYC. Available bulk rock Tmax
387 values for LV09, BB5, and HYC samples are consistent with biomarker-
388 based maturity parameters, supporting the indigenous nature of the
389 extracted hydrocarbons. Additionally, HI decreases with increasing
390 Rc(MPDF). No correlation between maturity and TOC was observed (R^2 =
391 0.13). Unmineralized HYC samples show slightly higher maturity levels in
392 comparison with previously published bitumens from the HYC ore body
393 (Williford et al., 2011). This pattern may be related to varying thermal
394 maturities in different mine locations.
395
396 *5.2. Potential controlling factors for $\delta^{13}C$ and $\delta^{2}H$ of* n-*alkanes*

397 The isotopic composition of *n*-alkanes in source rocks or reservoirs
398 potentially can be affected by a number of processes including thermal
399 maturity, hydrocarbon migration, oil mixing, water washing, biodegradation
400 and evaporative fractionation (e.g., Pedentchouk and Turich, 2018). In the
401 current study, in order to minimize in-reservoir fractionation effects, we
402 analysed extracted indigenous bitumens directly from the Barney Creek Fm
403 source rock instead of oil samples. Consequently, water washing,
404 evaporative fractionation and mix of several oils from multiple sources can

405 be excluded as dominant controlling factors for $\delta^{13}C_{alk}$ and $\delta^{2}H_{alk}$ variability.
406 Biodegradation can also be eliminated for the Barney Creek Fm bitumens
407 based on the relative abundance and distribution of *n*-alkanes (Fig. 2 and
408 Pawlowska et al., 2013). Instead, significant linear correlations of average
409 $\delta^{13}C_{alk}$ and $\delta^{2}H_{alk}$ with Rc(MPDF) (Fig. 4) suggest that thermal maturity is
410 the major factor that controls changes in the isotopic composition of the
411 Barney Creek Fm bitumens. Mechanisms of maturity control on $\delta^{13}C_{alk}$ and
412 $\delta^{2}H_{alk}$ will be discussed below.
413
414 *5.3. Stable hydrogen isotopes*
415 *5.3.1. Maturity control on $\delta^{2}H$ of n-alkanes in previous studies*
416 Under geological time and temperature, the primary hydrogen isotopic
417 composition of lipids can be strongly modified by diagenetic hydrogen
418 exchange processes and kinetic fractionation during thermal cracking
419 (Sessions, 2016). The effects of these two processes on hydrogen isotopes
420 might be hard to distinguish in natural samples, since both of them lead to
421 ^{2}H-enrichment. To exclude the impact of hydrogen exchange reactions with
422 water and only determine the effects of kinetic fractionation, Tang et al.
423 (2005) performed anhydrous, closed-system pyrolysis experiments on North
424 Sea petroleum and isolated *n*-alkanes from that oil. The study demonstrated
425 that *n*-alkanes became heavier in ^{2}H by 53‰ with increasing maturity from
426 0.9% to 1.5% of vitrinite reflectance equivalent. Several Phanerozoic field-
427 based studies are consistent with these results and illustrate an increase of

428 average δ^2H_{alk} by up to ~71‰ with rising maturity (Table 4) (e.g., Li et al.,
429 2001; Dawson et al., 2005, 2007; Radke et al., 2005; Maslen et al., 2012).
430 Additionally, heating rate might influence the extent of $^2H_{alk}$-enrichment.
431 For example, Radke et al. (2005) observed that in normal burial settings
432 with maturity ranging from Rc(MPI) = 0.65% to 1.26%, δ^2H_{alk} increased by
433 up to 52‰ for samples from the Permian Kupferschiefer, Poland. By
434 contrast, the Jurassic Posidonia Shale from Germany, affected by heating
435 from a magmatic intrusion, experienced a greater $^2H_{alk}$-enrichment by up to
436 67‰ in the smaller maturity range of Rc(MPI) = 0.64–1.04% (Radke et al.,
437 2005).
438
439 *5.3.2. δ^2H of* n-*alkanes in the Barney Creek Fm*
440 In the current study, hydrogen isotopes of *n*-alkanes in the immature to
441 early mature LV09 bitumens vary in the typical range for marine source
442 rocks with average δ^2H_{alk} between –103‰ and –120‰ (Sessions, 2016).
443 Analysed samples show an increase in δ^2H values with increasing *n*-alkane
444 carbon number (Fig. 3b, Table 3). Samples #3, #6, #8 and #9 exhibit the
445 most prominent "isotope slope" with up to 42‰ difference between low and
446 high molecular weight *n*-alkanes. Such an effect has been associated with
447 kinetic fractionation during thermal cracking (Tang et al., 2005).
448 Observation of this pattern in LV09 bitumens indicates that the isotope
449 slope may already become pronounced in samples of relatively low maturity
450 with Rc(MPDF) < 0.7%. Tang et al. (2005) also observed in their heating

451 experiments a steepening of the δ^2H isotope slope with increasing thermal
452 maturity from Rc = 0.9% to 1.5%. However, in the Barney Creek Fm, we
453 detect no steepening effect in the maturity range of Rc(MPDF) = 0.56–1.1%
454 (Fig. 3b). It is unclear whether the most mature sample with Rc(MPDF) =
455 1.24% shows an increase in slope, since the δ^2H_{alk} measurements for this
456 sample are available only for a limited range of *n*-alkanes (Fig. 3b, HYC
457 #20). Therefore, we cannot verify whether steepening of the δ^2H isotope
458 slope observed in pyrolysis experiments at the highest thermal maturities
459 also occurs in natural bitumens of the Barney Creek Fm.
460 Barney Creek Fm bitumens from several drill cores demonstrate an
461 increase of average δ^2H_{alk} by 69‰ as maturity rises from Rc(MPDF) = 0.56%
462 to 1.24% (Fig. 4d). However, the actual $^2H_{alk}$ enrichment might be even
463 higher because the long-chain *n*-alkanes, which are generally isotopically
464 heavier, could not be measured for the most mature sample (Fig. 3b). We
465 also included published δ^2H values for HYC ore body bitumens in Fig. 4.
466 Williford et al. (2011) reported that HYC ore body *n*-alkanes are enriched in
467 ^2H by up to 50–60‰ relative to *n*-alkanes from unmineralized, immature
468 Barney Creek Fm sediments from the GR-10 core distal from the mine. The
469 authors interpreted this apparently anomalous offset as a result of hydrogen
470 exchange with the mineralizing fluid during ore genesis. However, we
471 observe similar δ^2H values in ore body bitumens and bitumens from
472 sediments of similar burial maturity not affected by hydrothermal alteration
473 (BB5, BB6, and unmineralized HYC samples), negating the evidence for

474 anomalous $^{2}H_{alk}$ enrichment in the ore body (Fig. 4d). The isotopic offset is
475 fully consistent with a general $^{2}H_{alk}$ enrichment caused by increasing
476 thermal maturity. The magnitude of average isotopic enrichment in the
477 Barney Creek Fm is consistent with previously published empirical data
478 from field-based studies on Phanerozoic sequences (Table 4).
479 Fig. 5a compares correlations of average $\delta^{2}H_{alk}$ with maturity for Barney
480 Creek Fm bitumens and an artificially heated Phanerozoic crude oil sample
481 analysed by Tang et al. (2005). Even though Barney Creek Fm samples are
482 shifted by ~20‰ to heavier values of $\delta^{2}H_{alk}$, maturity-related trends of
483 average $\delta^{2}H_{alk}$ for both datasets experience almost the same slope (Fig. 5a).
484 In principle, the observed trend of increasing average $\delta^{2}H_{alk}$ with increasing
485 maturity in the Barney Creek Fm may reflect a combination of kinetic
486 fractionation caused by thermal cracking and hydrogen exchange effects.
487 However, since Tang et al. (2005) record a similar $^{2}H_{alk}$ enrichment under
488 exclusion of hydrogen exchange reactions, the data from the current study
489 may be solely explained by fractionation during thermal cracking.
490
491 *5.4. Stable carbon isotopes*
492 *5.4.1. Maturity control on $\delta^{13}C$ of n-alkanes in previous studies*
493 Although it is widely accepted that thermal maturity influences the
494 carbon isotopic composition of oils and *n*-alkanes, the precise mechanisms of
495 such fractionation effects are not fully understood. According to Clayton
496 (1991), oil generation and oil to gas cracking lead to increased $\delta^{13}C$ of

497 residual bitumen caused by $^{13}C/^{12}C$ kinetic fractionation. Preferential
498 breaking of $^{12}C–^{12}C$ bonds rather than $^{13}C–^{12}C$ bonds releases ^{13}C-depleted
499 compounds and results in ^{13}C-enrichment of the remaining oil fraction
500 (Clayton, 1991; Clayton and Bjorøy, 1994).

501 Previously published maturity-dependent $\delta^{13}C$ measurements of *n*-
502 alkanes in experimental and field-based studies are summarised in Table 4.
503 In the pyrolysis experiments on North Sea oil and isolated *n*-alkanes by
504 Tang et al. (2005), mentioned in Section 5.3.1, the average carbon isotopic
505 composition of *n*-alkanes increased by 4.6‰ with increasing maturity from
506 0.9% to 1.5% vitrinite reflectance equivalent. In a similar experimental
507 study, Tian et al. (2017) observed 5.5‰ average ^{13}C-enrichment for $C_{14–}C_{33}$
508 *n*-alkanes in anhydrous closed-system pyrolysis experiments at 250 °C to
509 450 °C on an oil sample from the Maoming Basin in China, and 6.6‰ for the
510 *n*-$C_{16–}C_{23}$ range (computed using data from Table 2 in Tian et al. (2017)).
511 Cheng et al. (2015) performed pyrolysis experiments on two immature
512 source rock samples from the Pearl River Mouth Basin in China and
513 recorded enrichment of average $\delta^{13}C_{alk}$ by 3.3‰ (Enping Fm) and 5.7‰
514 (Wenchang Fm) in the maturity range of Rc = 0.64–1.24%.

515 There are few published Phanerozoic field-based studies that report
516 systematic changes in $\delta^{13}C_{alk}$ with increasing maturity (Table 4) (e.g.,
517 Clayton and Bjorøy, 1994; Odden et al., 2002; Dawson et al., 2007; Cheng et
518 al., 2015). For instance, Clayton and Bjorøy (1994) in a study of Jurassic
519 North Sea oils showed an increase of average $\delta^{13}C_{alk}$ by 2.1‰ based on four

samples in the narrow maturity range of Rc(MPI) = 0.77–0.86%. Dawson et al. (2007) analysed 15 Upper Jurassic bitumens from the Vulcan sub-Basin in northern Australia with a wider maturity range of Ro = 0.7–1.6% and recorded a ~4.5‰ enrichment of average $\delta^{13}C_{alk}$ (estimated from Fig. 3 in Dawson et al. (2007)). In one available Precambrian study with possible maturity influence on $\delta^{13}C_{alk}$, Jarret et al. (2019) examined 12 bitumens from the Mesoproterozoic Velkerri Fm, Australia, in the maturity range Rc(MPDF) = 0.54–1.16% and observed a maximum increase of average $\delta^{13}C_{alk}$ by up to 3‰. However, due to noticeable scatter in the data and absence of a clear correlation with maturity, the authors suggested that organic matter source might represent a greater control on $\delta^{13}C_{alk}$ variations than thermal alteration.

5.4.2. $\delta^{13}C$ of n-alkanes in the Barney Creek Fm

Immature to early mature samples from the LV09 drill core presumably most closely reflect the primary $\delta^{13}C$ values of Barney Creek Fm *n*-alkyl lipids. Average $\delta^{13}C_{alk}$ of extracted bitumens vary from –30.6‰ to –31.8‰. As a comparison, these values are ~3‰ enriched relative to *n*-alkanes of similar maturity from the overlying 1.38 Ga Velkerri Fm in the McArthur Basin (Jarrett et al., 2019). In the absence of terrestrial higher plants or detectable eukaryotic algae, the $\delta^{13}C_{alk}$ values of these Paleo- and Mesoproterozoic successions predominantly reflect bacterial biomass (e.g., Brocks, 2018; Gueneli et al., 2018). Analysed samples demonstrate an

543 "inverse" isotopic ordering with ^{13}C-enrichment of extractable *n*-alkanes
544 relative to kerogen and positive values of $\Delta\delta^{13}C_{alk-ker}$ between 1.3‰ and
545 2.6‰ (Fig. 6c). Such inverse isotopic pattern is common in the Proterozoic
546 but is opposite to typical isotopic ordering in the Phanerozoic (Fig. 6a,b), a
547 difference likely related to fundamental transformations in the ecology of
548 primary producers and heterotrophs through time (Logan et al., 1995; Close
549 et al., 2011).

550 Barney Creek Fm bitumens from several drill cores demonstrate an
551 increase of average $\delta^{13}C_{alk}$ by up to 6.8‰ with increasing Rc(MPDF) from
552 0.44% to 1.3% (Fig. 4c). Over that maturity range, $\delta^{13}C_{ker}$ values stay
553 relatively constant (Fig. 4b, Table 1). Therefore, the isotopic offset $\Delta\delta^{13}C_{alk-ker}$, which reaches 8.5‰ in the most thermally altered sample (Fig. 4a, Fig.
555 6c), is controlled by variations in *n*-alkanes and not the kerogen. To our
556 knowledge, this is currently the highest recorded $^{13}C_{alk}$-enrichment caused
557 by thermal maturation. Even though our results show ~2–4‰ greater $^{13}C_{alk}$-
558 enrichment than other available field-based studies (Table 4, Section 5.4.1),
559 a meaningful comparison of the Paleoproterozoic Barney Creek Fm with
560 Phanerozoic field data is not possible at present.

561 High maturity-dependent $^{13}C_{alk}$-enrichment has not yet been recorded in
562 the limited published Phanerozoic field-based studies, several of which
563 examine only narrow maturity ranges. However, the observed increase of
564 $\delta^{13}C_{alk}$ values with rising thermal maturity in the Barney Creek Fm is
565 similar to the pyrolysis experiments by Tang et al. (2005) and Cheng et al.

(2015) on Phanerozoic oil and source rocks (compare slopes in Fig. 5b). In principle, since these experimental studies were performed on Phanerozoic oil and source rocks, $\delta^{13}C_{alk}$ in Phanerozoic natural environments could be affected by thermal alteration to the same extent. Thus, it is generally important to consider possible extreme $\delta^{13}C_{alk}$ alterations upon maturation in environmental studies and oil-source rock correlations for both Proterozoic and Phanerozoic sequences. The Barney Creek Fm case study also highlights a substantial thermal maturity impact on $\Delta\delta^{13}C_{alk–ker}$ values (Fig. 6c). Therefore, Precambrian community and redox reconstructions using $\Delta\delta^{13}C_{alk–ker}$ isotopic offsets (e.g., Logan et al., 1995; Close at al., 2011) must take thermal maturity into account.

5.4.3. Possible mechanisms for $^{13}C_{alk}$-enrichment and the "isotope slope"

The precise mechanisms responsible for the increase of average $\delta^{13}C_{alk}$ with increasing thermal maturity are unresolved. One commonly discussed mechanism suggests that the carbon isotopic enrichment is caused by kinetic fractionation associated with the breaking of C–C bonds along the carbon chain of *n*-alkanes (e.g., Clayton, 1991). Due to preferential homolytic cleavage of $^{12}C–^{12}C$ bonds over $^{13}C–^{12}C$, the thermal cracking of an *n*-alkane should generate two isotopically depleted shorter chain *n*-alkanes, resulting in relative enrichment of the intact residue of the parent *n*-alkane. According to Clayton (1991), this enrichment has a proportionally larger effect on residual short chain *n*-alkanes than higher homologues, leading to

589 progressive increase of $\delta^{13}C_{alk}$ with decreasing carbon number, creating a
590 negative "isotope slope". The emergence of negative isotope profiles during
591 increasing maturity was originally suggested by Silverman (1967) and later
592 developed by Clayton (1991). However, the proposed mechanism does not
593 account for changes in degradation rates with increasing carbon number.
594 For example, the rate constant k_h for homolytic cleavage of *n*-alkanes in a
595 radical chain reaction in the gas phase increases with chain length
596 (Watanabe et al., 2001). As a consequence, long chain *n*-alkanes degrade
597 faster than short chain homologues, resulting in faster enrichment of high
598 molecular-weight compounds (Tang et al., 2005). This effect could be further
599 enhanced by the addition of generated, isotopically depleted breakdown
600 products to the short chain *n*-alkane pool. Thus, according to Tang et al.
601 (2005), thermal cracking should lead to progressive ^{13}C (and ^{2}H) isotopic
602 enrichment of *n*-alkanes with rising carbon number, creating a positive, not
603 a negative, isotope slope. In their anhydrous pyrolysis experiments, Tang et
604 al. (2005) observed a steepening of the $\delta^{2}H_{alk}$ isotope slope with increasing
605 maturity. However, the predicted positive isotope slope in $\delta^{13}C_{alk}$ was not
606 detected. Based on comparison with $\delta^{2}H_{alk}$, the most mature pyrolysate (Rc
607 = 1.5%) should have displayed a carbon isotopic difference of 1.4‰ between
608 *n*-C_{13} and *n*-C_{21}. The authors argued that the expected positive $\delta^{13}C_{alk}$ slope
609 was not observed due to low analytical precision of the measurements
610 causing scattered $\delta^{13}C_{alk}$ values.

While Tang et al. (2005) performed pyrolysis experiments on bitumen and isolated *n*-alkanes, Cheng et al. (2015) pyrolysed immature source rock samples, thus observing the combined effect of *n*-alkane generation from kerogen and *n*-alkane cracking. In these experiments, $\delta^{13}C_{alk}$ slopes started to increase at Rc > 0.79%. An increase of the $\delta^{13}C_{alk}$ isotope slope was also detected in natural bitumens of the Enping Fm (Cheng et al., 2015), while in other published field-based studies the isotope slope either experienced no change (Odden et al., 2002; Cheng et al., 2015 for Wenchang Fm) or rotated to less positive values at higher maturities (Clayton and Bjorøy, 1994; Dawson et al., 2007).

In the current study, Barney Creek Fm bitumens display an inversion of the $\delta^{13}C_{alk}$ isotope slope from positive to negative with rising maturity (Figs. 3a and 7). The least mature Barney Creek Fm bitumens (drill core LV09) show slightly increasing positive isotope slopes within the maturity range of Rc(MPDF) = 0.44–0.71% (Fig. 7, $R^2 = 0.52$, $p = 0.008$). However, as maturity increases further from Rc(MPDF) = 0.9% to 1.3%, and the distributions of *n*-alkanes shift towards lower chain lengths due to near complete destruction of longer molecules (Fig. 2), the $\delta^{13}C_{alk}$ isotope slopes start to flatten and then become more negative (Figs. 3a and 7). Thus, cleavage of *n*-alkanes in radical chain reactions, which should generate increasingly positive isotope slopes (Tang et al., 2005), may not be the sole mechanism of ^{13}C-enrichment, and other reactions need to be considered.

634 *5.4.4. Simulation of $\delta^{13}C$ isotope slope behaviour*

635 To explore the formation of positive and negative $\delta^{13}C_{alk}$ isotope slopes
636 during organic matter maturation, we ran simple numerical models for
637 three mechanisms: (1) *n*-alkane cleavage in a radical chain reaction, (2)
638 reactions where the rate constant has limited dependence on the *n*-alkane
639 chain, and (3) generation of *n*-alkanes through degradation of kerogen. We
640 do not imply that the particular reaction mechanisms in the models play a
641 dominant role in *n*-alkane isotope slope formation in natural systems.
642 Rather, the aim is to explore principal reaction characteristics that may be
643 responsible for the generation of positive and negative slopes.

644 Fig. 8a shows the progression of $\delta^{13}C$ profiles during cleavage of *n*-
645 alkanes in a radical chain reaction in the gas-phase. In this model, *n*-
646 alkanes are cleaved by β-scission, generating two shorter-chain *n*-alkane
647 products that are isotopically depleted and returned to the *n*-alkane pool,
648 and the intact residues of the parent compounds become isotopically
649 enriched. Longer chain *n*-alkanes are cleaved considerably faster than
650 shorter homologues as the rate constant increases with chain length *n*
651 following $k_h \sim (n-2)(n-3)^{1/2}$ (Watanabe et al., 2001). We applied a $^{13}C/^{12}C$
652 fractionation factor $\alpha_h = 0.994$, a conservative estimate for homolytic mid-
653 chain cleavage of *n*-alkanes (Tang et al., 2000), although the precise value is
654 not critical for the purpose of the simulation. The isotopic values of all *n*-
655 alkanes at the start of the reaction were set to $\delta^{13}C = -32‰$. After 20
656 iterations of arbitrary time units, 98.1% of *n*-alkanes in the range C_{13} to C_{31}

were degraded, achieving an average isotopic enrichment comparable to the Barney Creek Fm. Moreover, as predicted by Tang et al. (2005) but unlike the Barney Creek Fm, the isotopic profiles develop increasingly positive isotope slopes (Fig. 8a). According to Tang et al. (2005), two effects with unknown relative importance contribute to the progressively increasing $\delta^{13}C_{alk}$ slopes: (1) generation of isotopically depleted breakdown products that are added to the short chain *n*-alkane pool, and (2) higher rate constants k_h for longer chain *n*-alkanes. To determine the relative importance of these effects, we adjusted the model to discard the cleavage products rather than returning them to the *n*-alkane pool. Surprisingly, the removal of ^{13}C-depleted products had only minimal impact on $^{13}C_{alk}$ enrichment. For instance, in the specific simulation shown in Fig. 8a, after 20 iterations *n*-C_{13} becomes enriched by 3.78‰ if isotopically depleted products are removed, and by 3.41‰ if they are returned to the *n*-alkane pool. Moreover, withdrawal of the breakdown products had no visible influence on isotope slopes. Therefore, effect (1) is unimportant for the trajectory of $\delta^{13}C$ profiles in a radical chain reaction, and the formation of the positive isotope slope can be largely attributed to the dependence of the rate constant k on chain length n.

The second model examines the evolution of $\delta^{13}C$ profiles during hypothetical reactions where the rate constant k_i has only a weak dependence on *n*-alkane chain length, or where short chain *n*-alkanes may even react faster than longer homologues. For bitumen degradation under

natural conditions, the dependence of rate constants on chain-lengths remains largely unexplored, so it is unclear which mechanisms have such characteristics. Plausible mechanisms include cracking and isomerization reactions where the reaction rate is controlled by access to limited sites on catalytic surfaces, or fast reactions in gas solution that favour homologues with lower evaporation energies. As an example, the simulation in Fig. 8b keeps k_i constant with chain length. As $^{13}C/^{12}C$ fractionation factors α_i of such reactions, to our knowledge, have not been determined, we chose $\alpha_i = 0.994$ to make the simulation comparable to the radical chain reaction in Fig. 8a. After 20 iterations of arbitrary time units, 99.96% of *n*-alkanes in the range C_{13} to C_{31} were degraded, again achieving an average isotopic enrichment comparable to the Barney Creek Fm. Without changes in k_i with increasing carbon number, the enrichment of residual *n*-alkanes is now proportionally larger for short-chain homologues than for longer homologues as described by Clayton (1991). Consequently, and in contrast to the radical chain reaction, the isotopic profiles develop increasingly negative isotope slopes (Fig. 8b).

To test whether competition between reactions with strong and weak dependence of k on n can reproduce the *n*-alkane abundances and isotope profiles of the Barney Creek Fm, we performed a simulation using actual *n*-alkane concentrations and isotope data for one of the least mature samples #02 (Fig. 8c). In the model, as an arbitrary choice, both reaction types ran in parallel at the same average reaction rates but with different fractionation

703 factors. Fig. 8c–d compares the model results with actual $\delta^{13}C$ data and *n*-
704 alkane abundance profiles of the Barney Creek Fm. Juxtaposition of the
705 plots reveals that the magnitude of the isotope effect, the inversion of the
706 isotope slope from positive to negative, the magnitude of decline in absolute
707 *n*-alkane abundances as well as the shift of *n*-alkane carbon numbers
708 towards lower molecular weight compounds were satisfactorily captured.
709 However, formation of the increasingly positive isotope slopes in the earliest
710 stages of maturation (Fig. 7, LV09 samples) was not captured. It is plausible
711 that the positive isotope slopes in LV09 samples formed during the early
712 stages of *n*-alkane generation (rather than degradation) through cleavage of
713 *n*-alkyl moieties from kerogen as illustrated in Fig. 9. In this model, the
714 inversion of the isotope slope from positive to negative is caused by the
715 exhaustion of *n*-alkyl moieties in the kerogen and a shift from *n*-alkane
716 formation to *n*-alkane degradation.
717 As mentioned, the numerical models shown in Figs. 8 and 9 do not imply
718 that the progression of *n*-alkane abundances and isotopes in the Barney
719 Creek Fm, or any other natural system, were caused by these specific
720 chemical mechanisms with the given rate constants and fractionation
721 factors. Rather, the models suggest that the dependence of the rate constant
722 *k* on chain length *n*, and the competition between *n*-alkane generation and
723 degradation, may be the dominant drivers for *n*-alkane isotope slope
724 behaviour. Therefore, future studies should aim to determine *k(n)* for
725 competing reactions in natural systems. More sophisticated models will

need to include numerous effects that were excluded here, such as generation of *n*-alkanes from functionalized *n*-alkyl lipids, temperature dependencies of rate constants and isotope fractionation factors, the generation of *n*-alkanes through cleavage of methylalkanes, alkyl aromatics and similar compounds, and isotope effects associated with the expulsion of *n*-alkanes from source rocks.

6. Conclusions

Immature to early mature Paleoproterozoic Barney Creek Fm samples from LV09 drill core show ^{13}C-enrichment of extractable *n*-alkanes relative to kerogen, thus following an inverse isotopic pattern that was previously observed in Precambrian formations (Logan et al., 1995). The δ^2H_{alk} values vary in the typical range for marine source rocks and become greater with increasing chain length of *n*-alkanes. The presence of this δ^2H_{alk} positive isotope slope demonstrates that kinetic fractionation effects already become evident at relatively low thermal maturities of Rc(MPDF) < 0.7%.

Compound-specific carbon and hydrogen isotope values of Barney Creek Fm *n*-alkanes from several drill cores correlate significantly with maturity, demonstrating a ^{13}C and ^{2}H enrichment of *n*-alkanes by up to 6.8‰ and 69‰ respectively with increasing maturity from Rc(MPDF) = 0.4% to 1.3%. The carbon isotopic offset $\Delta\delta^{13}C_{alk-ker}$, which reaches 8.5‰ in the most mature bitumen, is controlled by variations in *n*-alkanes rather than the kerogen, since $\delta^{13}C_{ker}$ values stay relatively constant. The greater extent of

749 $^{13}C_{alk}$-enrichment for Barney Creek Fm samples compared with available
750 Phanerozoic empirical data may reflect the limited number of published
751 studies about the thermal maturity influence on $\delta^{13}C_{alk}$. However, based on
752 similar trends of increasing isotopic enrichment with maturity in pyrolysis
753 experiments on Phanerozoic oils and source rocks, the isotopic composition
754 of *n*-alkanes in Phanerozoic and Precambrian sequences might be affected
755 by thermal alteration to a similar extent. As the observed thermal effect on
756 $\delta^{13}C_{alk}$ and $\delta^{2}H_{alk}$ is high enough to have an impact on biological and
757 environmental interpretations, it is important to consider maturity in oil-
758 source rock correlations and ecological reconstructions for Proterozoic and
759 Phanerozoic sediments. In particular, since thermal alteration can
760 substantially affect the isotopic offset between *n*-alkanes and kerogen
761 ($\Delta\delta^{13}C_{alk–ker}$), and presumably between *n*-alkanes and acyclic isoprenoids, it
762 is crucial to take thermal maturity into account when isotope systematics
763 are used to reconstruct Precambrian biological communities and trophic
764 relationships.

765 In the Barney Creek Fm, the slope of $\delta^{13}C$ *n*-alkane profiles changes
766 from positive to negative with increasing thermal maturity. Based on simple
767 numerical simulations, we suggest that this slope behaviour is driven by the
768 balance of the formation of *n*-alkanes from kerogen and their subsequent
769 degradation, and the dependence of the degradation rate constant *k* on *n*-
770 alkane chain length *n*. Initial generation of *n*-alkanes from kerogen forms a
771 positive isotope slope. Degradation mechanisms where *k* strongly increases

with chain length, such as radical chain reactions, also cause positive isotope slopes, while mechanisms with a lower dependence on chain length result in negative isotope slopes. The changing importance of these competing reactions in the progression from early diagenesis to metagenesis may be responsible for the observed isotope slope inversion in the Barney Creek Fm and other systems.

Acknowledgements

We thank Janet Hope (ANU) for laboratory support. We are grateful to Jacob Sohn and Junhong Chen for technical assistance with isotope measurements and Ian Long for isolation of kerogen in the Organic Geochemistry Laboratory at Geoscience Australia (GA). We thank Michael Kipp (UW) for organic carbon isotope measurements and Ruslan Khamidullin (Lomonosov MSU) for help with Rock-Eval pyrolysis. We thank Darryl Stacey from the Darwin Core Library (NTGS), Neil Williams and McArthur River Mining Pty Ltd for access to drill cores. We are grateful to Alex L. Sessions and Ilya Bobrovskiy for reviewing an earlier version of this manuscript. This research was financially supported by Australian Research Council grants DP160100607 and DP170100556 (to JJB). GV acknowledges support from an Australian Government Research Training Program (RTP) Scholarship. AJMJ publishes with permission of the CEO, Geoscience Australia. The authors declare no conflicting interests, financial or otherwise. Daniel Dawson, Kenneth Peters, and two anonymous

795 reviewers are thanked for their thoughtful comments and suggestions,
796 which improved this manuscript. Andrew Murray and John Volkman are
797 thanked for editorial assistance.
798
799 *Associate Editor*–**Andrew Murray**
800
801 **References**
802 Ahmad, M., Dunster, J.N., Munson, T.J., 2013. Chapter 15: McArthur
803 Basin, In: Ahmad, M., Munson, T.J. (compilers), Geology and Mineral
804 Resources of the Northern Territory. Northern Territory Geological
805 Survey, Special Publication 5.
806 Alexander, R., Kagi, R.I., Larcher, A.V., 1982. Clay catalysis of aromatic
807 hydrogen-exchange reactions. Geochimica et Cosmochimica Acta 46,
808 219–222.
809 Brocks, J.J., 2011. Millimeter-scale concentration gradients of hydrocarbons
810 in Archean shales: Live-oil escape or fingerprint of contamination?
811 Geochimica et Cosmochimica Acta 75, 3196–3213.
812 Brocks, J.J., 2018. The transition from a cyanobacterial to algal world and
813 the emergence of animals. Emerging Topics in Life Sciences 2(2),
814 181–190.
815 Brocks, J.J., Grosjean, E., Logan, G.A., 2008. Assessing biomarker
816 syngeneity using branched alkanes with quaternary carbon (BAQCs)

817 and other plastic contaminants. Geochimica et Cosmochimica Acta
818 72, 871–888.
819 Brocks, J.J., Love, G.D., Summons, R.E., Knoll, A.H., Logan, G.A., Bowden,
820 S.A., 2005. Biomarker evidence for green and purple sulphur bacteria
821 in a stratified Palaeoproterozoic sea. Nature 437, 866–870.
822 Cheng, P., Xiao, X.M., Gai, H.F., Li, T.F., Zhang, Y.Z., Huang, B.J., Wilkins,
823 R.W.T., 2015. Characteristics and origin of carbon isotopes of n-
824 alkanes in crude oils from the western Pearl River Mouth Basin,
825 South China sea. Marine and Petroleum Geology 67, 217–229.
826 Clayton, C., 1991. Effect of maturity on carbon isotope ratios of oils and
827 condensates. Organic Geochemistry 17, 887–899.
828 Clayton, C., Bjorøy, M., 1994. Effect of maturity on $^{13}C/^{12}C$ ratios of
829 individual compounds in North Sea oils. Organic Geochemistry 21,
830 737–750.
831 Close, H.G., Bovee, R., Pearson, A., 2011. Inverse carbon isotope patterns of
832 lipids and kerogen record heterogeneous primary biomass. Geobiology
833 9, 250–265.
834 Dahl, B., Bojesen-Koefoed, J., Holm, A., Justwan, H., Rasmussen, E.,
835 Thomsen, E., 2004. A new approach to interpreting Rock-Eval S2 and
836 TOC data for kerogen quality assessment. Organic Geochemistry 35,
837 1461–1477.
838 Dawson, D., Grice, K., Alexander, R., 2005. Effect of maturation on the
839 indigenous δD signatures of individual hydrocarbons in sediments

and crude oils from the Perth Basin (Western Australia). Organic Geochemistry 36, 95–104.

Dawson, D., Grice, K., Alexander, R., Edwards, D., 2007. The effect of source and maturity on the stable isotopic compositions of individual hydrocarbons in sediments and crude oils from the Vulcan Sub-basin, Timor Sea, Northern Australia. Organic Geochemistry 38, 1015–1038.

Eldridge, C., Williams, N., Walshe, J.L., 1993. Sulfur isotope variability in sediment-hosted massive sulfide deposits as determined using the ion microprobe SHRIMP; II, A study of the HYC Deposit at McArthur River, Northern Territory, Australia. Economic Geology 88, 1–26.

Espitalié, J., Madec, M., Tissot, B., 1980. Role of mineral matrix in kerogen pyrolysis: influence on petroleum generation and migration. Bulletin of the American Association of Petroleum Geologists 64, 59–66.

French, K.L., Hallmann, C., Hope, J.M., Schoon, P.L., Zumberge, J.A., Hoshino, Y., Peters, C.A., George, S.C., Love, G.D., Brocks, J.J., Buick, R., Summons, R.E., 2015. Reappraisal of hydrocarbon biomarkers in Archean rocks. Proceedings of the National Academy of Sciences 112, 5915–5920.

Gueneli, N., McKenna, A., Ohkouchi, N., Boreham, C., Beghin, J., Javaux, E., Brocks, J., 2018. 1.1-billion-year-old porphyrins establish a marine ecosystem dominated by bacterial primary producers. Proceedings of the National Academy of Sciences 115, E6978–E6986.

862 Hayes, J.M., 2001. Fractionation of carbon and hydrogen isotopes in
863 biosynthetic processes. Reviews in Mineralogy and Geochemistry 43,
864 225–277.
865 Ireland, T., Large, R.R., McGoldrick, P., Blake, M., 2004. Spatial
866 distribution patterns of sulfur isotopes, nodular carbonate, and ore
867 textures in the McArthur River (HYC) Zn-Pb-Ag deposit, Northern
868 Territory, Australia. Economic Geology 99, 1687–1709.
869 Jackson, M., Muir, M.D., Plumb, K.A., 1987. Geology of the southern
870 McArthur Basin, Northern Territory (Vol. 220). Australian
871 Government Publishing Service, Canberra.
872 Jarrett, A.J.M., Cox, G.M., Brocks, J.J., Grosjean, E., Boreham, C.J.,
873 Edwards, D.S., 2019. Microbial assemblage and palaeoenvironmental
874 reconstruction of the 1.38 Ga Velkerri Formation, McArthur Basin,
875 northern Australia. Geobiology 17, 360–380.
876 Jarvie, D.M., 2012. Shale resource systems for oil and gas: Part 2—Shale oil
877 resource systems. In: Breyer, J. (Ed.), Shale reservoirs – Giant
878 resources for the 21st century. American Association of Petroleum
879 Geologists Memoir 97, 89–119.
880 Johnson, R., Bluett, J., Titus, L., Warner, D., 2013. Exploring and
881 appraising the oldest gas accumulations in Australia. The APPEA
882 Journal 53, 470–470.
883 Kipp, M.A., Stüeken, E.E., Yun, M., Bekker, A., Buick, R., 2018. Pervasive
884 aerobic nitrogen cycling in the surface ocean across the

885 Paleoproterozoic Era. Earth and Planetary Science Letters 500, 117–
886 126.
887 Kunzmann, M., Schmid, S., Blaikie, T.N., Halverson, G.P., 2019. Facies
888 analysis, sequence stratigraphy, and carbon isotope
889 chemostratigraphy of a classic Zn-Pb host succession: The Proterozoic
890 middle McArthur Group, McArthur Basin, Australia. Ore Geology
891 Reviews 106, 150–175.
892 Kvalheim, O.M., Christy, A.A., Telnæs, N., Bjørseth, A., 1987. Maturity
893 determination of organic matter in coals using the
894 methylphenanthrene distribution. Geochimica et Cosmochimica Acta
895 51, 1883–1888.
896 Li, M., Huang, Y., Obermajer, M., Jiang, C., Snowdon, L.R., Fowler, M.G.,
897 2001. Hydrogen isotopic compositions of individual alkanes as a new
898 approach to petroleum correlation: case studies from the Western
899 Canada Sedimentary Basin. Organic Geochemistry 32, 1387–1399.
900 Logan, G.A., Hayes, J., Hieshima, G.B., Summons, R.E., 1995. Terminal
901 Proterozoic reorganization of biogeochemical cycles. Nature 376, 53–
902 56.
903 Logan, G.A., Summons, R.E., Hayes, J.M., 1997. An isotopic biogeochemical
904 study of Neoproterozoic and Early Cambrian sediments from the
905 Centralian Superbasin, Australia. Geochimica et Cosmochimica Acta
906 61, 5391–5409.

907 Maslen, E., Grice, K., Dawson, D., Wang, S., Horsfield, B., 2012. Stable
908 hydrogen isotopes of isoprenoids and *n*-alkanes as a proxy for
909 estimating the thermal history of sediments through geological time.
910 In: Analyzing the Thermal History of Sedimentary Basins: Methods
911 and Case Studies. Society for Sedimentary Geology Special
912 Publication 103, 29–43.
913 Munson, T., 2016. Sedimentary Characterisation of the Wilton Package,
914 Greater MacArthur Basin, Northern Territory. Northern Territory
915 Geological Survey, Record 2016-003.
916 Murray, A.P., Summons, R.E., Boreham, C.J., Dowling, L.M., 1994.
917 Biomarker and *n*-alkane isotope profiles for Tertiary oils: relationship
918 to source rock depositional setting. Organic Geochemistry 22, 521–
919 IN526.
920 Odden, W., Barth, T., Talbot, M., 2002. Compound-specific carbon isotope
921 analysis of natural and artificially generated hydrocarbons in source
922 rocks and petroleum fluids from offshore Mid-Norway. Organic
923 Geochemistry 33, 47–65.
924 Page, R.W., Sweet, I.P., 1998. Geochronology of basin phases in the western
925 Mt Isa Inlier, and correlation with the McArthur Basin. Australian
926 Journal of Earth Sciences 45, 219–232.
927 Pawlowska, M.M., Butterfield, N.J., Brocks, J.J., 2013. Lipid taphonomy in
928 the Proterozoic and the effect of microbial mats on biomarker
929 preservation. Geology 41, 103–106.

930 Pedentchouk, N., Freeman, K.H., Harris, N.B., 2006. Different response of
931 δD values of *n*-alkanes, isoprenoids, and kerogen during thermal
932 maturation. Geochimica et Cosmochimica Acta 70, 2063–2072.
933 Pedentchouk, N., Turich, C., 2018. Carbon and hydrogen isotopic
934 compositions of *n*-alkanes as a tool in petroleum exploration.
935 Geological Society, London, Special Publications 468, 105–125.
936 Peters, K., 1986. Guidelines for evaluating petroleum source rock using
937 programmed pyrolysis. Bulletin of the American Association of
938 Petroleum Geologists 70, 318–329.
939 Peters, K., Walters, C., Moldowan, J., 2005. The Biomarker Guide: Volume
940 2, Biomarkers and Isotopes in Petroleum Exploration and Earth
941 History. Cambridge University Press.
942 Peters, K.E., Cassa, M.R., 1994. Applied source rock geochemistry. In:
943 Magoon, L.B., Dow, W.G. (Eds.). The Petroleum System—From
944 Source to Trap. American Association of Petroleum Geologists
945 Memoir 60, pp. 93–120.
946 Powell, T.G., Jackson, M.J., Sweet, I.P., Crick, I.H., Boreham, C.J.,
947 Summons, R.E., 1987. Petroleum geology and geochemistry, middle
948 Proterozoic McArthur Basin. Bureau of Mineral Resources Record 48,
949 286.
950 Radke, J., Bechtel, A., Gaupp, R., Püttmann, W., Schwark, L., Sachse, D.,
951 Gleixner, G., 2005. Correlation between hydrogen isotope ratios of

952 lipid biomarkers and sediment maturity. Geochimica et
953 Cosmochimica Acta 69, 5517–5530.
954 Rooney, M., Vuletich, A., Griffith, C., 1998. Compound-specific isotope
955 analysis as a tool for characterizing mixed oils: an example from the
956 West of Shetlands area. Organic Geochemistry 29, 241–254.
957 Schimmelmann, A., Lewan, M.D., Wintsch, R.P., 1999. D/H isotope ratios of
958 kerogen, bitumen, oil, and water in hydrous pyrolysis of source rocks
959 containing kerogen types I, II, IIS, and III. Geochimica et
960 Cosmochimica Acta 63, 3751–3766.
961 Schinteie, R., Brocks, J.J., 2017. Paleoecology of Neoproterozoic hypersaline
962 environments: Biomarker evidence for haloarchaea, methanogens,
963 and cyanobacteria. Geobiology 15, 641–663.
964 Schinteie, R., Colangelo-Lillis, J.R., Hope, J.M., Chen, J., Nelson, D.B.,
965 Jarrett, A.J., Brocks, J.J., 2019. Impact of drill core contamination on
966 compound-specific carbon and hydrogen isotopic signatures. Organic
967 Geochemistry 128, 161–171.
968 Sessions, A.L., 2016. Factors controlling the deuterium contents of
969 sedimentary hydrocarbons. Organic Geochemistry 96, 43–64.
970 Sessions, A.L., Sylva, S.P., Summons, R.E., Hayes, J.M., 2004. Isotopic
971 exchange of carbon-bound hydrogen over geologic timescales.
972 Geochimica et Cosmochimica Acta 68, 1545–1559.

973 Silverman, S.R., 1967. Carbon isotopic evidence for the role of lipids in
974 petroleum formation. Journal of the American Oil Chemists' Society
975 44, 691–695.
976 Stüeken, E.E., 2013. A test of the nitrogen-limitation hypothesis for
977 retarded eukaryote radiation: nitrogen isotopes across a
978 Mesoproterozoic basinal profile. Geochimica et Cosmochimica Acta
979 120, 121–139.
980 Tang, Y., Huang, Y., Ellis, G.S., Wang, Y., Kralert, P.G., Gillaizeau, B., Ma,
981 Q., Hwang, R., 2005. A kinetic model for thermally induced hydrogen
982 and carbon isotope fractionation of individual *n*-alkanes in crude oil.
983 Geochimica et Cosmochimica Acta 69, 4505–4520.
984 Tang, Y., Perry, J., Jenden, P., Schoell, M., 2000. Mathematical modeling of
985 stable carbon isotope ratios in natural gases. Geochimica et
986 Cosmochimica Acta 64, 2673–2687.
987 Tian, C., Xia, Y., Song, C., Ma, S., Gao, W., Xing, L., 2017. Changes in the
988 carbon isotope composition of pristane and phytane with increasing
989 maturity. Petroleum Science and Technology 35, 1270–1276.
990 van Maldegem, L.M., 2017. Molecular and isotopic signatures of life
991 surrounding the Neoproterozoic Snowball Earth events. Ph.D.
992 Dissertation, Universität Bremen.
993 Vinnichenko, G., Jarrett, A.J.M., Hope, J.M., Brocks, J.J., 2020. Discovery of
994 the oldest known biomarkers provides evidence for phototrophic

bacteria in the 1.73 Ga Wollogorang Formation, Australia. Geobiology 18, 544–559.

Watanabe, M., Adschiri, T., Arai, K., 2001. Overall rate constant of pyrolysis of *n*-alkanes at a low conversion level. Industrial & Engineering Chemistry Research 40, 2027–2036.

Williford, K.H., Grice, K., Logan, G.A., Chen, J., Huston, D., 2011. The molecular and isotopic effects of hydrothermal alteration of organic matter in the Paleoproterozoic McArthur River Pb/Zn/Ag ore deposit. Earth and Planetary Science Letters 301, 382–392.

Figure captions

Fig. 1. McArthur Basin in northern Australia with location of the drill cores investigated in this study.

Fig. 2. Total ion chromatograms (TIC) of saturated fractions and separated *n*-alkanes for Barney Creek Fm samples (a) #9 and (b) #22 of different maturity. Black circles represent *n*-alkanes. Pr: pristane; Ph: phytane; IS: internal standard, co-eluting with *n*-C_{24}.

Fig. 3. (a) $\delta^{13}C$ of *n*-alkanes and (b) $\delta^{2}H$ of *n*-alkanes from the Barney Creek Formation plotted against chain length.

Fig. 4. Plots of calculated vitrinite reflectance Rc(MPDF) for Barney Creek Formation extracted bitumens vs (a) carbon isotopic offset between *n*-alkanes and kerogen ($\Delta\delta^{13}C_{alk-ker}$), (b) carbon isotopes of kerogen ($\delta^{13}C_{ker}$), (c) average $\delta^{13}C$ of *n*-alkanes and (d) average $\delta^{2}H$ of *n*-alkanes. In addition to the R^2 values, we added Spearman's ρ and the corresponding p value because of non-normal distribution of the data. Note that previously published CSIA and $\delta^{13}C_{ker}$ values for HYC samples are included in the correlations (Williford et al., 2011).

Fig. 5. Comparison between maturity-related CSIA trends for Barney Creek Formation bitumens from the current study and artificially heated Phanerozoic crude oil sample (Tang et al., 2005) and source rocks (Cheng et al., 2015). The plots show calculated vitrinite reflectance Rc against (a) average $\delta^{2}H$ of *n*-alkanes and (b) average $\delta^{13}C$ of *n*-alkanes. Since the maturity of the unheated Phanerozoic oil sample is unknown in the experiments by Tang et al. (2005), here we provide CSIA measurements for the range of Rc = 0.9–1.5%. m: slope from linear equations.

Fig. 6. Schematic carbon isotope signatures of *n*-alkanes relative to kerogen for (a) Phanerozoic sediments, which are typically in agreement with the biosynthetic fractionation pattern (Hayes, 2001); and (b) Proterozoic sediments demonstrating an "inverse" isotopic ordering (Logan et al, 1995, 1997). (c) Whisker plots illustrating maturity effect on $\delta^{13}C$ of *n*-alkanes

relative to kerogen in the Paleoproterozoic Barney Creek Formation. n = 12 in Rc = 0.4–0.7%, n = 11 in Rc = 0.9–1.1%, n = 3 in Rc = 1.2–1.3%.

Fig. 7. Carbon "isotope slope" inversion with increasing calculated vitrinite reflectance Rc(MPDF) for Barney Creek Formation extracted bitumens. Isotope slope values for each sample were obtained from plots of $\delta^{13}C$ of n-alkanes against chain length (Fig. 3a). The full range of available carbon numbers was used for the computation of slope values. P values were calculated for R^2.

Fig. 8. Comparison of measured and simulated n-alkane concentrations and $\delta^{13}C$ values. (a) Simulated progression of $\delta^{13}C$ for n-alkanes with increasing maturation during cleavage of n-alkanes to shorter n-alkanes in a gas-phase radical chain reaction where the rate constant follows $k_h \sim (n-2)\times(n-3)^{1/2}$ (where n is chain length). At the end of the reaction, 1.9% of n-C_{13} to n-C_{31} remain. (b) Simulation of isomerization or degradation of n-alkanes where the rate constant k_i is independent of chain length and the reaction products are not returned to the n-alkane pool. At the end of the reaction, 0.04% of n-C_{13} to n-C_{31} remain. (c) Simulation of maturation based on actual n-alkane concentrations and $\delta^{13}C$ isotope data for Barney Creek Fm sample #02 (t = 1). In the simulation, the two reaction types shown in (a) and (b) were run simultaneously. At the end of the reaction, 1.8% of n-C_{13} to n-C_{31} remain. (d) Actual Barney Creek Fm data for six selected samples within the isotopic

1064 shift spectrum. The drop in absolute concentrations of *n*-alkanes (*n*-C_{13} to *n*-
1065 C_{31}) relative to TOC from the least (#02) to most mature (#21) Barney Creek
1066 Fm sample in the plot is 98.6%, i.e. 1.4% of initial concentrations remain.
1067 Model parameters are given in the Supplementary Information.
1068
1069 **Fig. 9.** Simulation of generation of *n*-alkanes from kerogen and
1070 simultaneous *n*-alkane degradation following the two mechanisms in Fig.
1071 8c. Model parameters are given in the Supplementary Information.

Figure 1

Click here to access/download;Figure;Figure 1.tif

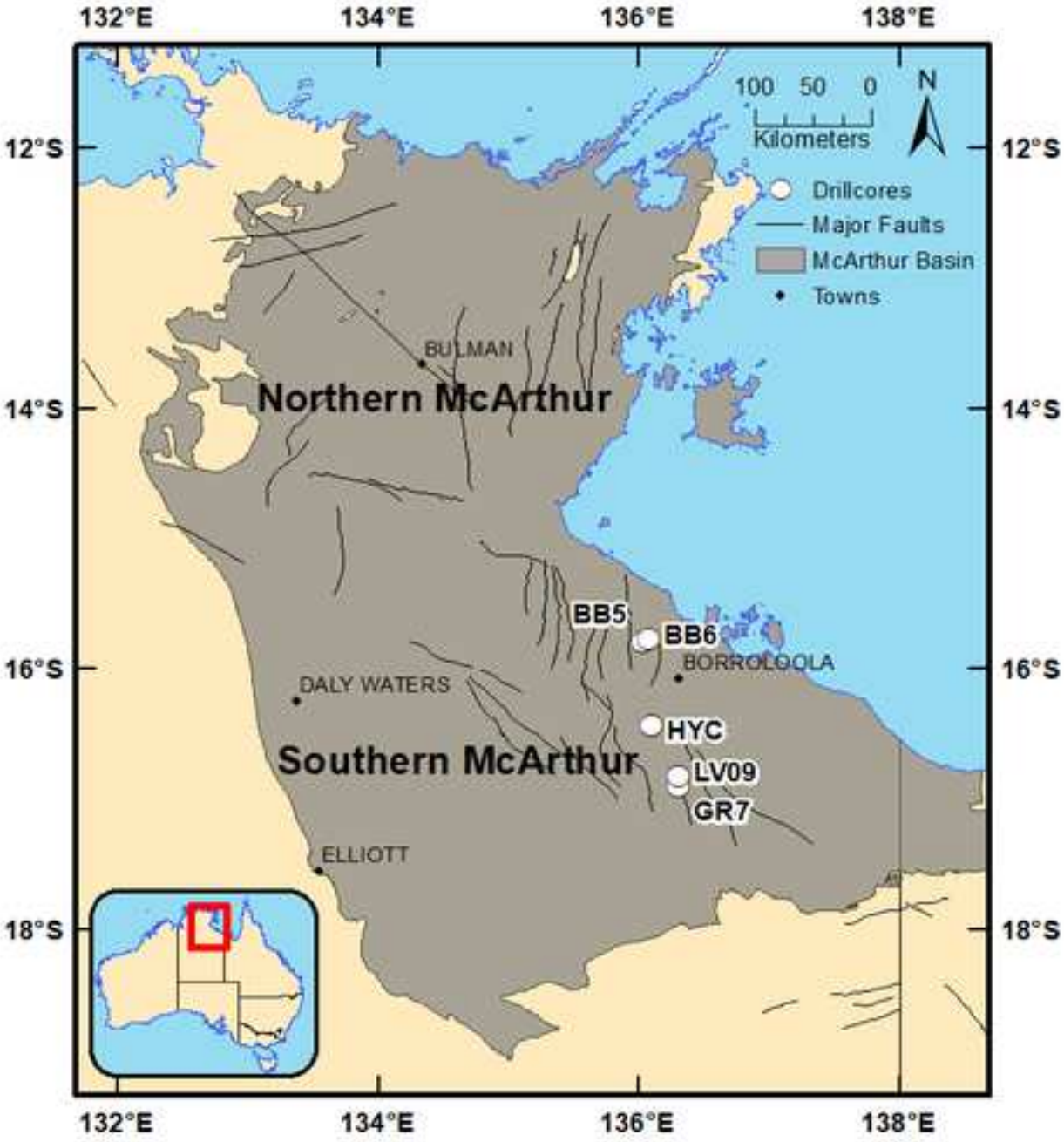

Figure 2

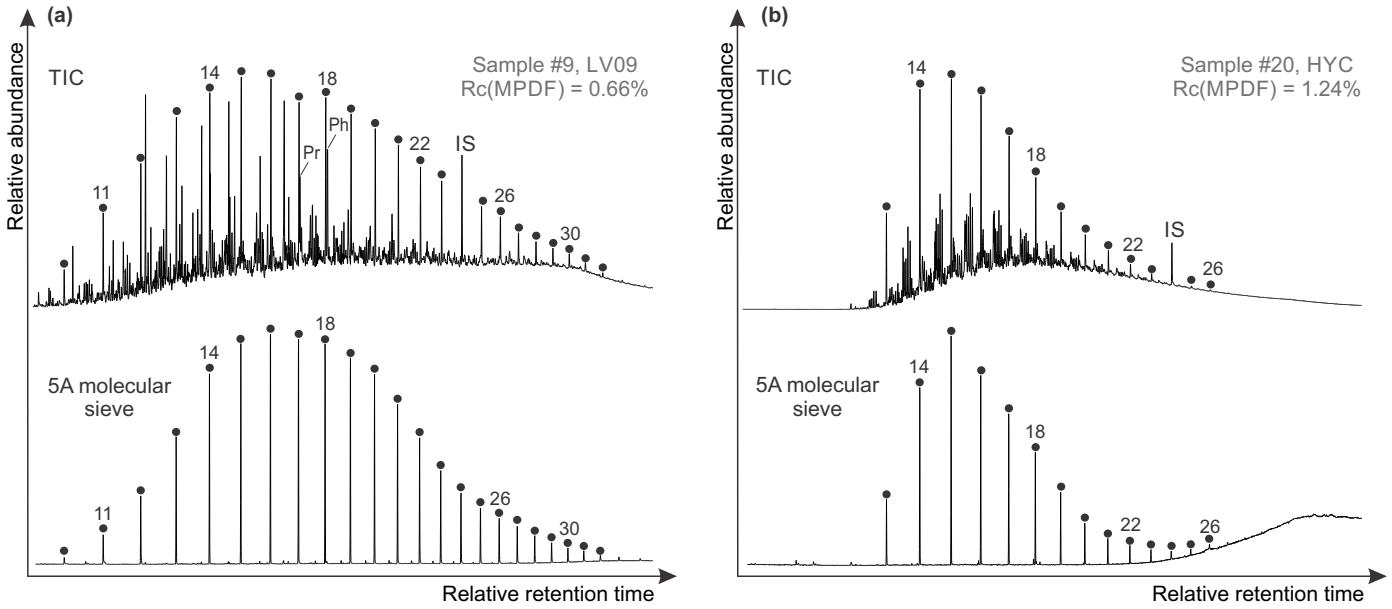

Figure 3

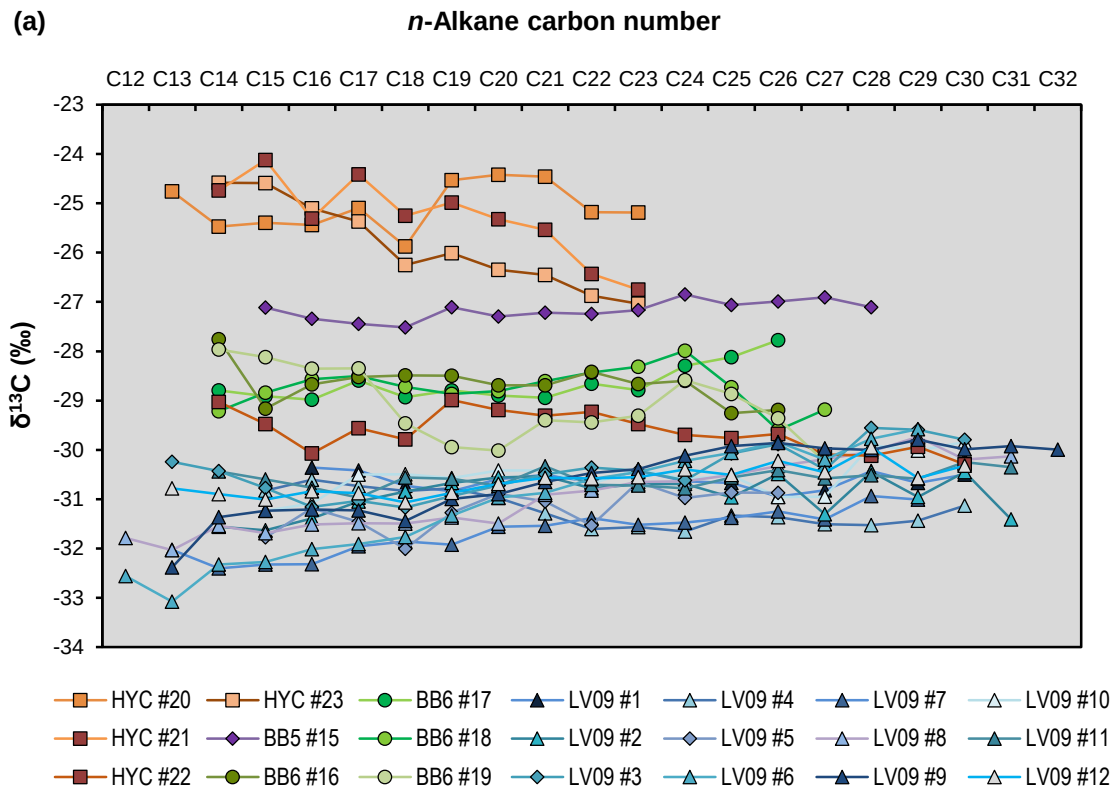

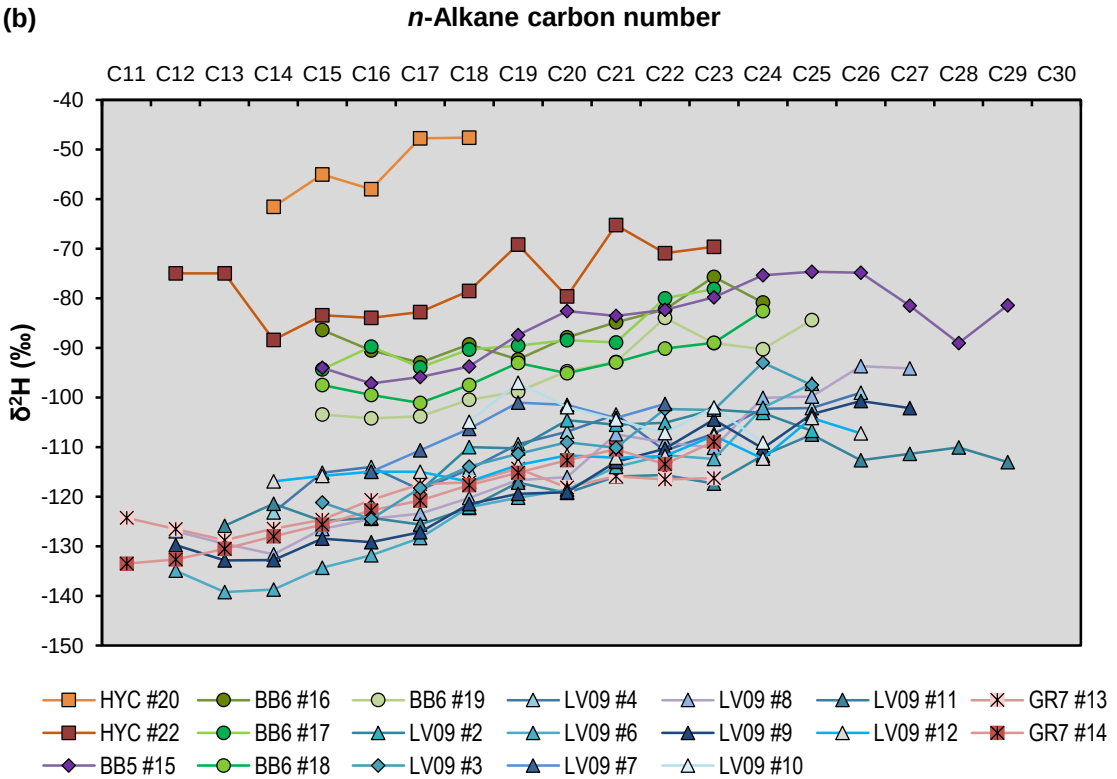

Figure 4

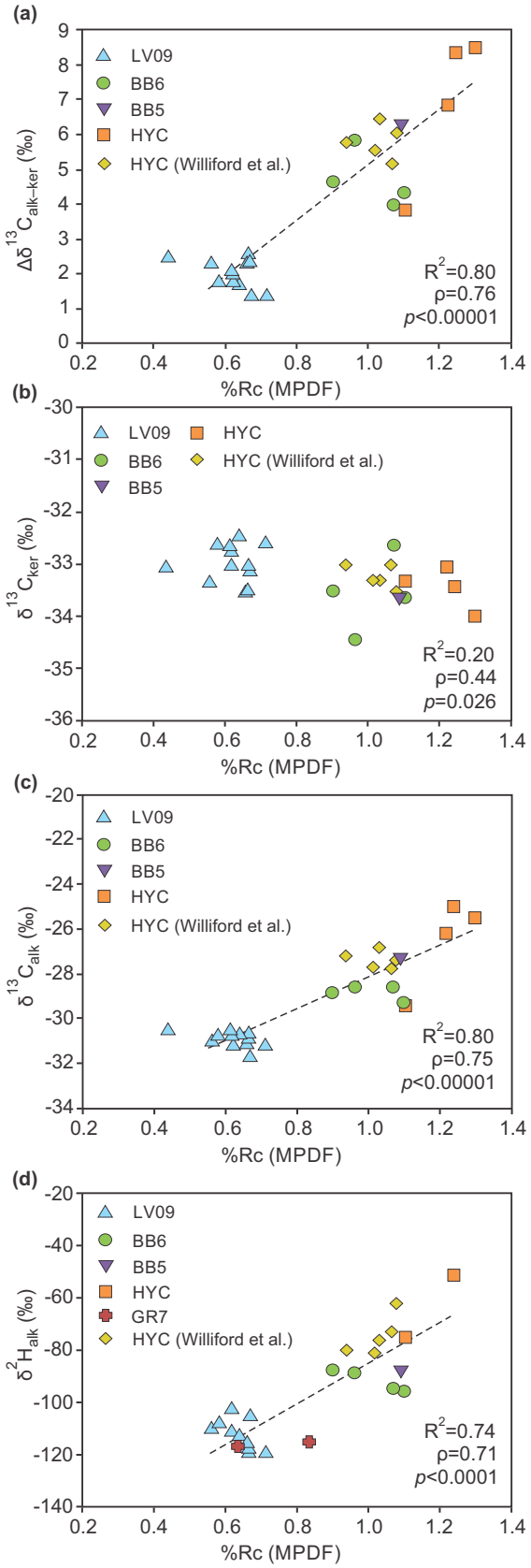

Figure 5

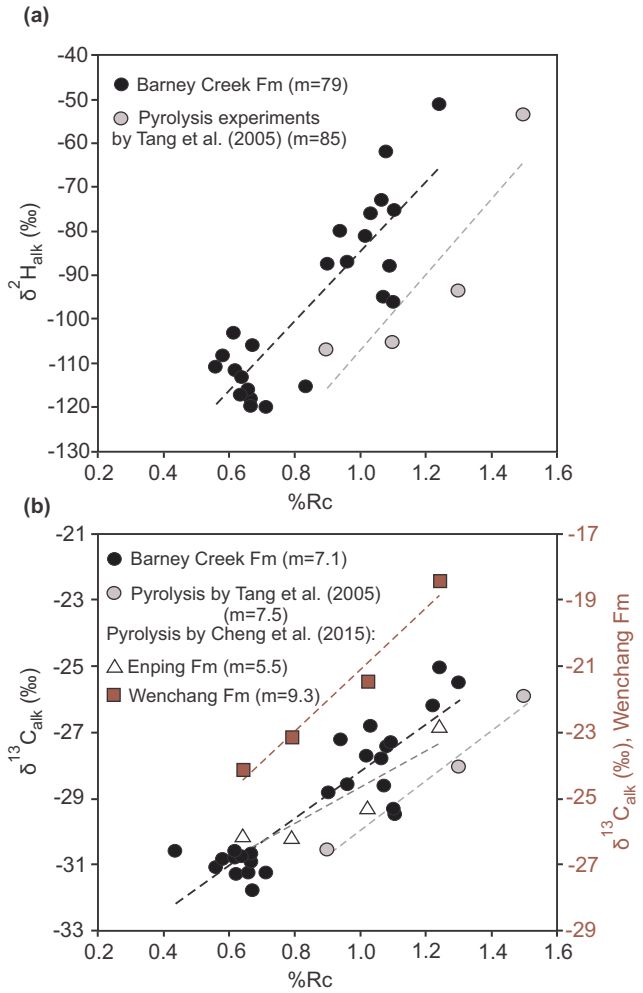

Figure 6

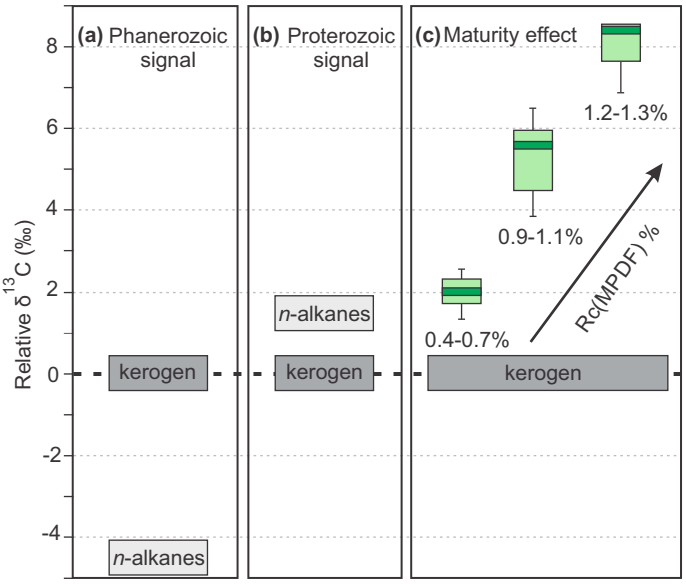

Figure 7

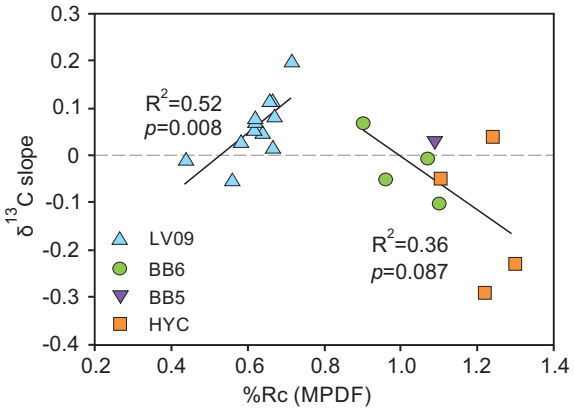

Figure 8

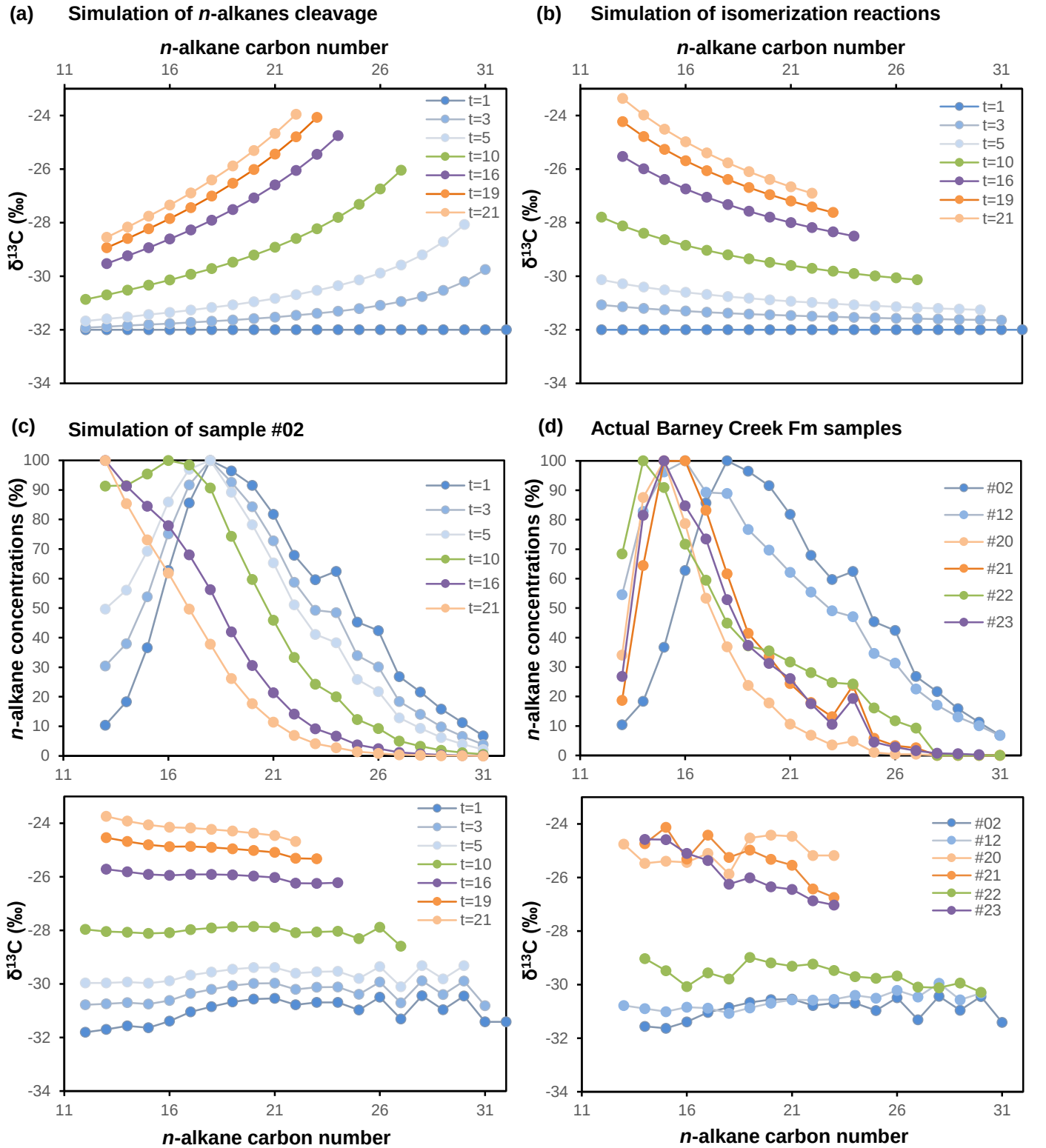

Figure 9

Click here to access/download;Figure;Figure 9.pptx

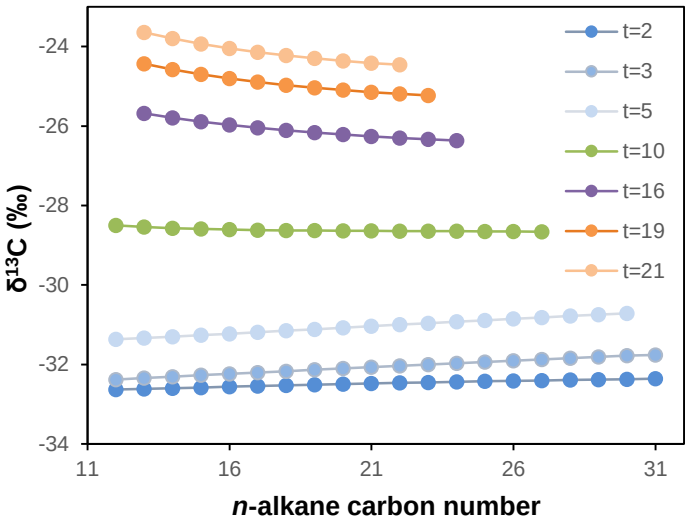

Table 1. Thermal maturity, TOC, Rock-Eval pyrolysis parameters and isotope ratios of Barney Creek Formation samples

Sample ID	Drill core[a]	Depth (m)	MPDF[b]	Rc (MPDF)[c]	Tmax[d] (°C)	TOC[e] (%)	S1[f]	S2[g]	PI[h]	S1/ TOC[i]	HI[j]	$\delta^{13}C$ ker[k] (‰)	$\delta^{13}C$ alk[l] (‰)	$\Delta\delta^{13}C_{alk-ker}$[m] (‰)	$\delta^{2}H$ alk[n] (‰)
#1	LV09	414.75	0.27	0.44	430	1.12	0.36	3.85	0.09	32	344	-33.1	-30.6	2.5	n.d.
#2	LV09	429.7	0.33	0.58	433	1.57	0.78	7.32	0.10	50	466	-32.6	-30.8	1.8	-108
#3	LV09	450.0	0.35	0.62	435	2.26	1.32	10.73	0.11	58	475	-32.8	-30.8	2.0	-112
#4	LV09	461.83	0.32	0.56	431	2.23	1.02	9.30	0.10	46	417	-33.4	-31.1	2.4	-111
#5	LV09	470.7	0.35	0.62	424	0.87	0.38	3.46	0.10	44	398	-33.0	-31.3	1.7	n.d.
#6	LV09	477.0	0.39	0.71	434	4.36	2.69	22.35	0.11	62	513	-32.6	-31.3	1.4	-120
#7	LV09	478.2	0.37	0.67	431	0.60	0.14	1.61	0.08	23	268	-33.1	-31.8	1.3	-106
#8	LV09	485.0	0.37	0.66	438	4.71	2.50	24.24	0.09	53	515	-33.5	-31.2	2.3	-116
#9	LV09	489.0	0.37	0.66	435	3.78	1.82	17.0	0.10	48	450	-33.5	-30.9	2.6	-118
#10	LV09	494.5	0.35	0.61	436	0.45	0.06	0.73	0.08	13	162	-32.7	-30.6	2.1	-103
#11	LV09	494.6	0.37	0.67	433	3.26	1.56	13.26	0.11	48	407	-33.0	-30.7	2.3	-120
#12	LV09	498.88	0.36	0.63	427	3.38	1.88	12.12	0.13	56	359	-32.5	-30.8	1.7	-113
#13	GR7	683.54	0.36	0.64	-	-	-	-	-		-	-	-	-	-117
#14	GR7	869.6	0.45	0.83	-	-	-	-	-		-	-	-	-	-115
#15	BB5	215.8	0.56	1.09	442	2.23	0.20	0.41	0.33	9	18	-33.6	-27.3	6.3	-88
#16	BB6	108.9	0.50	0.96	n.d.	0.62	0.10	0.28	0.27	16	44	-34.4	-28.6	5.8	-87
#17	BB6	125.75	0.48	0.90	n.d.	1.03	0.22	0.66	0.25	21	64	-33.5	-28.8	4.7	-87
#18	BB6	134.5	0.55	1.07	n.d.	1.09	0.27	0.67	0.29	25	61	-32.6	-28.6	4.0	-95
#19	BB6	142.67	0.56	1.10	n.d.	1.07	0.21	0.66	0.24	20	62	-33.6	-29.3	4.3	-96
#20	BS024-01	16.4	0.63	1.24	443	2.99	0.19	0.67	0.22	6	22	-33.4	-25.0	8.4	-51
#21	BS024-01	41.5	0.65	1.30	463	1.44	0.03	0.29	0.09	2	20	-34.0	-25.5	8.5	n.d.
#22	BS024-01	105.1	0.57	1.10	446	0.42	0.02	0.14	0.13	5	33	-33.3	-29.5	3.8	-75
#23	MRM 2012-03	210.8	0.62	1.22	468	0.35	0.01	0.04	0.20	3	11	-33.1	-26.2	6.9	n.d.
#24*	HYC	Mine pit	0.55	1.08	n.d.	0.79	n.d.	n.d.	n.d.	n.d.	6	-33.5	-27.4	6.1	-62
#25*	HYC		0.55	1.06	n.d.	0.48	n.d.	n.d.	n.d.	n.d.	4	-33.0	-27.8	5.2	-73
#26*	HYC		0.53	1.02	n.d.	0.48	n.d.	n.d.	n.d.	n.d.	13	-33.3	-27.7	5.6	-81
#27*	HYC		0.53	1.03	n.d.	0.48	n.d.	n.d.	n.d.	n.d.	2	-33.3	-26.8	6.5	-76
#28*	HYC		0.49	0.94	n.d.	0.56	n.d.	n.d.	n.d.	n.d.	12	-33.0	-27.2	5.8	-80

[a]Drill core: LV09, GR7, BB5, BB6 – open source drill cores; BS024-01 and MRM 2012-03 are from the Here is Your Chance (HYC) mine. *#24–28: previously analysed Barney Creek Formation (BCF) samples from HYC (Williford et al., 2011).

[b]Methylphenanthrene distribution factor MPDF = (3-MP+2-MP)/(3-MP+2-MP+9-MP+1-MP) (Kvalheim et al., 1987).

[c]Calculated vitrinite reflectance Rc(MPDF) = 2.242×MPDF – 0.166 (Kvalheim et al., 1987). [d]Temperature at maximum of S2 peak. [e]Total organic carbon (%) from Rock-Eval pyrolysis. [f]Free hydrocarbons, mg HC/g rock. [g]Generative potential, mg HC/g rock. [h]Production index PI = S1/(S1+S2). [i]Oil saturation index = (S1/TOC)×100 mg HC/g TOC. [j]Hydrogen index HI = S2*100/TOC in mg HC/g TOC. [k]Organic carbon isotope values of kerogen. [l]Stable carbon isotopic composition of *n*-alkanes (average of *n*-$C_{16–23}$ for the current study and of *n*-$C_{18–21}$ for samples #24–28). [m]*n*-alkane–kerogen isotopic offset. [n]Stable hydrogen isotopic composition of *n*-alkanes (average of *n*-$C_{16–23}$ for the current study and of *n*-$C_{18–C21}$ for samples #23–27). n.d. – not detectable or unreliable. "-" – not measured.

Table 2. *n*-Alkane carbon isotopic composition of Barney Creek Formation bitumens

ID	δ¹³C (‰), carbon number																			
	12	13	14	15	16	17	18	19	20	21	22	23	24	25	26	27	28	29	30	31
#1	n.d.	n.d.	n.d.	n.d.	-30.4 (0)	-30.4 (0.3)	-30.7 (0)	-30.8 (0.2)	-30.6 (0.1)	-30.5 (0.1)	-30.7 (0.1)	-30.4 (0.1)	-30.6 (0.1)	-30.7 (0)	-31.0 (0.2)	-30.8 (0.2)	-30.4 (0.1)	-30.7 (0.2)	-30.5 (0.1)	n.d.
#2	n.d.	n.d.	-31.6 (0)	-31.6 (0.1)	-31.4 (0.1)	-31.0 (0.1)	-30.9 (0.1)	-30.7 (0.1)	-30.6 (0.1)	-30.5 (0)	-30.8 (0.1)	-30.7 (0.2)	-30.7 (0.3)	-31.0 (0)	-30.5 (0.1)	-31.3 (0.3)	-30.4 (0)	-31.0 (0)	-30.5 (0.1)	-31.4 (0.3)
#3	n.d.	-30.2 (0.1)	-30.4 (0)	-30.8 (0.3)	-31.2 (0.3)	-31.0 (0.2)	-31.2 (0.2)	-30.9 (0.2)	-30.7 (0.2)	-30.5 (0.3)	-30.4 (0.2)	-30.4 (0.1)	-30.6 (0.2)	-30.1 (0.1)	-29.9 (0.3)	-30.4 (0.1)	-29.6 (0.3)	-29.6 (0.2)	-29.8 (0.1)	n.d.
#4	n.d.	n.d.	n.d.	-30.8 (0.2)	-30.6 (0.3)	-30.7 (0.3)	-30.8 (0.3)	-30.8 (0.3)	-31.0 (0.3)	-31.3 (0.1)	-31.6 (0)	-31.6 (0.1)	-31.7 (0)	-31.3 (0)	-31.4 (0.1)	-31.5 (0.2)	-31.5 (0.3)	-31.4 (0.2)	-31.1 (0.4)	n.d.
#5	n.d.	n.d.	n.d.	-31.8 (0.1)	-31.2 (0)	-31.5 (0.2)	-32.0 (0)	-31.3 (0)	-30.9 (0.1)	-31.1 (0.2)	-31.5 (0.2)	-30.7 (0.1)	-31.0 (0.2)	-30.9 (0.3)	-30.9 (0.1)	n.d.	n.d.	n.d.	n.d.	n.d.
#6	-32.6 (0)	-33.1 (0.1)	-32.3 (0.1)	-32.3 (0.1)	-32.0 (0.2)	-31.9 (0.1)	-31.8 (0)	-31.3 (0)	-31.0 (0.1)	-30.9 (0)	-30.6 (0)	-30.5 (0)	-30.2 (0.1)	-30.1 (0)	-29.8 (0.2)	-30.2 (0.4)	-29.8 (0.3)	-29.6 (0.1)	n.d.	n.d.
#7	n.d.	-32.0 (0.1)	-32.4 (0.1)	-32.3 (0.1)	-32.3 (0.1)	-32.0 (0.1)	-31.9 (0.1)	-31.9 (0)	-31.6 (0.1)	-31.5 (0.1)	-31.4 (0)	-31.5 (0.1)	-31.5 (0.1)	-31.4 (0)	-31.3 (0.3)	-31.4 (0.2)	-30.9 (0.2)	-31.0 (0.2)	n.d.	n.d.
#8	-31.8 (0)	-32.0 (0)	-31.5 (0.2)	-31.7 (0.1)	-31.5 (0)	-31.5 (0)	-31.5 (0.1)	-31.4 (0.1)	-31.5 (0.1)	-30.9 (0)	-30.8 (0.1)	-30.7 (0.2)	-30.6 (0.4)	-30.5 (0.5)	-30.3 (0.3)	-30.2 (0.5)	-30.0 (0)	-29.7 (0.1)	-30.2 (0.3)	-30.1 (0.3)
#9	n.d.	-32.4 (0.3)	-31.4 (0.1)	-31.2 (0.1)	-31.2 (0)	-31.2 (0)	-31.4 (0.1)	-31.0 (0)	-31.0 (0)	-30.7 (0)	-30.5 (0)	-30.4 (0)	-30.1 (0)	-29.9 (0.1)	-29.9 (0)	-30.0 (0)	-30.0 (0.1)	-29.8 (0)	-30.0 (0.1)	-29.9 (0.2)
#10	n.d.	n.d.	n.d.	-31.2 (0.3)	-31.1 (0)	-30.5 (0.2)	-30.5 (0.1)	-30.6 (0)	-30.4 (0)	-30.4 (0.1)	-30.7 (0.1)	-30.4 (0.2)	-30.6 (0.1)	-30.5 (0.2)	-31.0 (0.1)	-31.0 (0.3)	-29.9 (0.2)	-30.0 (0.1)	-29.8 (0.2)	n.d.
#11	n.d.	n.d.	-30.4 (0.1)	-30.6 (0.1)	-30.8 (0.1)	-31.0 (0.3)	-30.6 (0.2)	-30.6 (0.1)	-30.7 (0.2)	-30.3 (0.1)	-30.7 (0.1)	-30.7 (0.1)	-30.8 (0)	-30.6 (0)	-30.4 (0.3)	-30.6 (0.3)	-30.5 (0.2)	-30.6 (0.1)	-30.3 (0.1)	-30.4 (0)
#12	n.d.	-30.8 (0)	-30.9 (0.2)	-31.0 (0.1)	-30.8 (0)	-30.9 (0)	-31.1 (0)	-30.9 (0)	-30.7 (0)	-30.6 (0)	-30.6 (0.1)	-30.6 (0.1)	-30.4 (0.3)	-30.5 (0.1)	-30.2 (0)	-30.5 (0.3)	-30.0 (0.2)	-30.6 (0)	-30.3 (0.3)	n.d.
#13	n.d.	n.d.	n.d.	n.d.	n.d.	n.d.	n.d.	n.d.	n.d.	n.d.	n.d.	n.d.	n.d.	n.d.	n.d.	n.d.	n.d.	n.d.	n.d.	n.d.
#14	n.d.	n.d.	n.d.	n.d.	n.d.	n.d.	n.d.	n.d.	n.d.	n.d.	n.d.	n.d.	n.d.	n.d.	n.d.	n.d.	n.d.	n.d.	n.d.	n.d.
#15	n.d.	n.d.	n.d.	-27.1 (0)	-27.3 (0.2)	-27.5 (0.3)	-27.5 (0.3)	-27.1 (0.1)	-27.3 (0.3)	-27.2 (0.3)	-27.3 (0.4)	-27.2 (0.3)	-26.9 (0.1)	-27.1 (0.2)	-27.0 (0)	-26.9 (0)	-27.1 (0.2)	n.d.	n.d.	n.d.
#16	n.d.	n.d.	-27.8 (0.1)	-29.2 (0.5)	-28.7 (0.3)	-28.5 (0.3)	-28.5 (0.3)	-28.5 (0.2)	-28.7 (0.2)	-28.7 (0.2)	-28.4 (0.1)	-28.7 (0)	-28.6 (0.3)	-29.3 (0.1)	-29.2 (0)	n.d.	n.d.	n.d.	n.d.	n.d.

#17	n.d.	n.d.	-28.8 (0)	-28.9 (0)	-29.0 (0)	-28.6 (0.1)	-28.9 (0.2)	-28.8 (0.3)	-28.9 (0.2)	-28.9 (0.2)	-28.7 (0.3)	-28.8 (0.4)	-28.3 (0.3)	-28.1 (0)	-27.8 (0.2)	n.d.	n.d.	n.d.	n.d.	n.d.
#18	n.d.	n.d.	-29.2 (0.1)	-28.8 (0)	-28.6 (0.1)	-28.5 (0)	-28.7 (0)	-28.9 (0.1)	-28.8 (0.1)	-28.6 (0.1)	-28.4 (0.1)	-28.3 (0.1)	-28.0 (0.1)	-28.7 (0.1)	-29.6 (0)	-29.2 (0)	n.d.	n.d.	n.d.	n.d.
#19	n.d.	n.d.	-28.0 (0.1)	-28.1 (0.1)	-28.4 (0.1)	-28.4 (0.1)	-29.5 (0.1)	-29.9 (0.4)	-30.0 (0.3)	-29.4 (0.4)	-29.4 (0.2)	-29.3 (0)	-28.6 (0.1)	-28.9	-29.4	-30.2	n.d.	n.d.	n.d.	n.d.
#20	n.d.	-24.8 (0.3)	-25.5 (0.5)	-25.4 (0.1)	-25.4 (0.2)	-25.1 (0.1)	-25.9 (0)	-24.5 (0.1)	-24.4 (0.1)	-24.5 (0.1)	-25.2 (0.2)	-25.2 (0.4)	n.d.	n.d.	n.d.	n.d.	n.d.	n.d.	n.d.	n.d.
#21	n.d.	n.d.	-24.7 (0.3)	-24.1 (0.2)	-25.3 (0.1)	-24.4 (0.2)	-25.3 (0)	-25.0 (0.4)	-25.3 (0.2)	-25.5 (0)	-26.4 (0.1)	-26.8 (0.2)	n.d.	n.d.	n.d.	n.d.	n.d.	n.d.	n.d.	n.d.
#22	n.d.	n.d.	-29.0 (0.4)	-29.5 (0.2)	-30.1 (0.1)	-29.6 (0.2)	-29.8 (0.1)	-29.0 (0.1)	-29.2 (0.1)	-29.3 (0)	-29.2 (0)	-29.5 (0.1)	-29.7 (0.1)	-29.8 (0.1)	-29.7 (0)	-30.1 (0.1)	-30.1 (0)	-29.9 (0)	-30.3 (0)	n.d.
#23	n.d.	n.d.	-24.6 (0.1)	-24.6 (0.2)	-25.1 (0.1)	-25.4 (0)	-26.3 (0.1)	-26.0 (0.2)	-26.4 (0.2)	-26.5 (0)	-26.9 (0.1)	-27.0 (0.2)	n.d.	n.d.	n.d.	n.d.	n.d.	n.d.	n.d.	n.d.

LV09: samples #1–12; GR7: samples #13 and 14; BB5: sample #15; BB6: samples #16–19; BS024-01: samples #20–22; MRM 2012-03: sample #23. n.d. – not detectable. Numbers in parentheses are standard deviations. No standard deviation value means the result is collected from a single run.

Table 3. *n*-Alkane hydrogen isotopic composition of Barney Creek Formation bitumens

ID	δ²H (‰), carbon number																		
	11	12	13	14	15	16	17	18	19	20	21	22	23	24	25	26	27	28	29
#1	n.d.	n.d.	n.d.	n.d.	n.d.	n.d.	n.d.	n.d.	n.d.	n.d.	n.d.	n.d.	n.d.	n.d.	n.d.	n.d.	n.d.	n.d.	n.d.
#2	n.d.	n.d.	n.d.	n.d.	n.d.	n.d.	-119(2)	-110(1)	-110(1)	-105(2)	-106(2)	-105(2)	-102(1)	-103(2)	-107(3)	n.d.	n.d.	n.d.	n.d.
#3	n.d.	n.d.	n.d.	n.d.	-121(2)	-125(1)	-118(0)	-114(2)	-111(5)	-109(5)	-110(3)	-102(0)	-103(1)	-93(2)	-98(3)	n.d.	n.d.	n.d.	n.d.
#4	n.d.	n.d.	n.d.	-123(1)	-115(0)	-114(5)	-119(3)	-115(2)	-109(1)	-107(3)	-103(4)	-111(3)	-107(5)	-102(3)	-102(1)	-99(4)	n.d.	n.d.	n.d.
#5	n.d.	n.d.	n.d.	n.d.	n.d.	n.d.	n.d.	n.d.	n.d.	n.d.	n.d.	n.d.	n.d.	n.d.	n.d.	n.d.	n.d.	n.d.	n.d.
#6	n.d.	-135(1)	-139(1)	-139(1)	-134(0)	-132(2)	-128(2)	-122(4)	-120(3)	-119(3)	-114(2)	-112(2)	-112(2)	-102(6)	-97(2)	n.d.	n.d.	n.d.	n.d.
#7	n.d.	n.d.	n.d.	n.d.	n.d.	-115(1)	-111(4)	-106(4)	-101(3)	-102(2)	-104(2)	-101(1)	n.d.	n.d.	n.d.	n.d.	n.d.	n.d.	n.d.
#8	n.d.	-127(2)	-130(0)	-132(1)	-127(1)	-124(1)	-123(1)	-120(1)	-117(2)	-116(0)	-107(1)	-109(0)	-110(3)	-100(3)	-100(4)	-94(1)	-94(0)	n.d.	n.d.
#9	n.d.	-130(1)	-133(1)	-133(2)	-129(0)	-129(1)	-127(3)	-122(1)	-119(2)	-119(1)	-113(1)	-110(1)	-105(2)	-110(1)	-103(5)	-101(3)	-102(2)	n.d.	n.d.
#10	n.d.	n.d.	n.d.	n.d.	n.d.	n.d.	n.d.	-105(1)	-97(1)	-102(0)	-104(1)	-107(3)	-102(2)	-109(0)	n.d.	n.d.	n.d.	n.d.	n.d.
#11	n.d.	n.d.	-126(1)	-121(1)	-125(2)	-124(2)	-126(2)	-122(3)	-117(3)	-119(2)	-116(1)	-116(1)	-117(2)	-112(2)	-108(3)	-113(1)	-111(2)	-110(1)	-113(0)
#12	n.d.	n.d.	n.d.	-117(2)	-116(2)	-115(1)	-115(3)	-117(1)	-114(4)	-112(2)	-112(3)	-112(2)	-108(4)	-112(1)	-104(1)	-107(1)	n.d.	n.d.	n.d.
#13	-124(1)	-127(1)	-129(1)	-126(2)	-125(3)	-121(2)	-118(2)	-117(0)	-114(2)	-118(1)	-116(2)	-117(1)	-116(1)	n.d.	n.d.	n.d.	n.d.	n.d.	n.d.
#14	-134(1)	-133(2)	-131(2)	-128(1)	-126(2)	-123(1)	-121(0)	-118(0)	-115(2)	-113(4)	-111(1)	-113(2)	-109(4)	n.d.	n.d.	n.d.	n.d.	n.d.	n.d.
#15	n.d.	n.d.	n.d.	n.d.	-94(4)	-97(5)	-96(5)	-94(5)	-87(2)	-83(3)	-84(3)	-82(3)	-80(3)	-75(2)	-75(5)	-75(1)	-82(0)	-89(1)	-81(0)
#16	n.d.	n.d.	n.d.	n.d.	-86(2)	-91(2)	-93(2)	-89(2)	-92(1)	-88(4)	-85(0)	-82(3)	-76(1)	-81(3)	n.d.	n.d.	n.d.	n.d.	n.d.
#17	n.d.	n.d.	n.d.	n.d.	-94(1)	-90(0)	-94(2)	-90(1)	-90(4)	-88(2)	-89(5)	-80(5)	-78(3)	n.d.	n.d.	n.d.	n.d.	n.d.	n.d.
#18	n.d.	n.d.	n.d.	n.d.	-98(1)	-100(1)	-101(0)	-98(3)	-93(2)	-95(1)	-93(4)	-90(2)	-89(5)	-83(2)	n.d.	n.d.	n.d.	n.d.	n.d.
#19	n.d.	n.d.	n.d.	n.d.	-103(1)	-104(1)	-104(1)	-101(1)	-99(0)	-95(0)	-93(1)	-84(4)	-89(2)	-90(0)	-84(3)	n.d.	n.d.	n.d.	n.d.
#20	n.d.	n.d.	n.d.	-62(1)	-55(3)	-58(2)	-48(3)	-48(3)	n.d.	n.d.	n.d.	n.d.	n.d.	n.d.	n.d.	n.d.	n.d.	n.d.	n.d.
#21	n.d.	n.d.	n.d.	n.d.	n.d.	n.d.	n.d.	n.d.	n.d.	n.d.	n.d.	n.d.	n.d.	n.d.	n.d.	n.d.	n.d.	n.d.	n.d.
#22	n.d.	-75(5)	-75(2)	-88(1)	-83(6)	-84(6)	-83(4)	-79(1)	-69(3)	-80(3)	-65(2)	-71(0)	-70(0)	n.d.	n.d.	n.d.	n.d.	n.d.	n.d.
#23	n.d.	n.d.	n.d.	n.d.	n.d.	n.d.	n.d.	n.d.	n.d.	n.d.	n.d.	n.d.	n.d.	n.d.	n.d.	n.d.	n.d.	n.d.	n.d.

LV09: samples #1–12; GR7: samples #13 and 14; BB5: sample #15; BB6: samples #16–19; BS024-01: samples #20–22; MRM 2012-03: sample #23. n.d. – not detectable. Numbers in parentheses are standard deviations.

Table 4. Summary of CSIA measurements for experimental and field-based studies

	Formation	Samples type	Age	Thermal maturity[a]	δ^2Halk increase[b]	δ^{13}Calk increase[c]	Reference
Experimental studies	North Sea	oil		T = 390–445 °C, Rc(T) = 0.9–1.5%	53‰ ($C_{16–21}$), n = 5	4.6‰ ($C_{16–21}$), n = 4	Tang et al., 2005
	Enping Fm, China	source rock	Oligocene	T = 300–380 °C, Rc(T) = 0.64–1.24%		3.3‰ ($C_{16–23}$), n = 4	Cheng et al., 2015
	Wenchang Fm, China	source rock	Eocene	T = 300–380 °C, Rc(T) = 0.64–1.24%		5.7‰ ($C_{16–23}$), n = 4	Cheng et al., 2015
	Youganwo Fm, China	oil	Eocene-Oligocene	T = 250–450 °C		5.5‰ ($C_{14–33}$); 6.6‰ ($C_{16–23}$), n = 6	Tian et al., 2017
Phanerozoic field-based studies	Enping Fm, China	bitumens	Oligocene	Increasing depth, 2550–4610 m		3‰ ($C_{16–23}$), n = 10	Cheng et al., 2015
	Wenchang Fm, China	bitumens	Eocene	Increasing depth, 3254–3394 m		2.8‰ ($C_{16–23}$), n = 6	Cheng et al., 2015
	North Sea	oils	Jurassic	Rc(MPI) = 0.77–0.86%		2.1‰ ($C_{16–23}$), n = 4	Clayton and Bjorøy, 1994
	Spekk Fm, Norway	bitumens	Late Jurassic	%Ro = 0.75–1.05		1.8‰ ($C_{16–23}$), n = 3	Odden et al., 2002
	Vulcan Fm, Australia	bitumens	Late Jurassic	Paqualin-1: %Ro = 0.7–1.6; Vulcan-1B: %Ro = 0.7–1.2%	Paqualin-1: ~28‰, n = 8; Vulcan-1B: ~36‰, n = 8; ($C_{13–31}$)	*Paqualin-1: ~4.5‰, n = 8; Vulcan-1B: ~2‰, n = 7	Dawson et al., 2007
	Posidonia Shale, Germany	bitumens	Early Jurassic	Rc(MPI) = 0.64–1.04%	67‰ ($C_{11–35}$); 68‰ ($C_{16–23}$), n = 4		Radke et al., 2005
	Kockatea shale, Australia	oils and bitumens	Early Triassic	Rc = 0.53–1.13%	42‰ ($C_{12–32}$), n = 9		Dawson et al., 2005
	Kupferschiefer Shale, Poland	bitumens	Late Permian	Rc(MPI) = 0.65–1.26%	52‰ ($C_{11–35}$); 71‰ ($C_{16–23}$), n = 8		Radke et al., 2005
	Duvernay Fm, Canada	bitumens	Upper Devonian	Rc(Tmax) = 0.38–0.78%	up to 71‰ ($C_{10–32}$), n = 4		Maslen et al., 2012
	Western Canada	oils	Ordovician–Cretaceous	increasing maturity	*up to 40‰, n = 5		Li et al., 2001
Precambrian field-based studies	Velkerri Fm, Australia	bitumens	Mesoproterozoic	Rc(MPDF) = 0.54–1.16%		up to 3‰ ($C_{16–23}$), n = 12	Jarrett et al., 2019
	Barney Creek Fm, Australia	bitumens	Paleoproterozoic	Rc(MPDF) = 0.44–1.3%	up to 68.8‰ ($C_{16–23}$), n = 19	up to 6.8‰ ($C_{16–23}$), n = 21	Current study

[a]Thermal maturity estimated with vitrinite reflectance (%Ro) and equivalent vitrinite reflectance (Rc) calculated from: T – temperature during pyrolysis experiments; Tmax – temperature at maximum of Rock-Eval S2 peak; MPI – methylphenanthrene index; MPDF – methylphenanthrene distribution factor. [b,c]Maximum enrichment in average hydrogen (^{2}H) or carbon (^{13}C) isotopic composition of *n*-alkanes with increasing maturity; the range of compounds is specified in parentheses. *n*: number of samples; *$\delta^{2}H$ or $\delta^{13}C$ data estimated from Figures.